Metamorphic paragenesis and P-T conditions in garnet amphibolite from the Median Segment of the Idefjorden Terrane, Lilla Edet

Anna Sartell

Dissertations in Geology at Lund University,
Bachelor's thesis, no 574
(15 hp/ECTS credits)

Department of Geology
Lund University
2019

Metamorphic paragenesis and P-T conditions in garnet amphibolite from the Göta Älv Shear Zone around Lilla Edet

Bachelor's thesis

Anna Sartell

Department of Geology
Lund University
2019

Contents

Cover Picture: Photo of the sample location, showing one of the north-west dipping garnet amphibolite bodies found by the railroad north of Hälltorp. The rock shows evidence of partial melting. Photo by Anna Sartell.

Metamorphic paragenesis and P-T conditions in garnet amphibolite from the Göta Älv Shear Zone around Lilla Edet

Anna Sartell

Sartell, A., 2019: Metamorphic paragenesis and P-T conditions in garnet amphibolite from the garnet amphibolite from the Göta Älv Shear Zone around Lilla Edet. *Dissertations in Geology at Lund University*, No. 574, 36 pp. 15 hp (15 ECTS credits) .

Abstract: The Sveconorwegian orogeny (c. 1 Ga) lead to the recrystallization of large parts of southwestern Sweden, with widespread metamorphism as well as local migmatization. The Idefjorden Terrane, which has been studied less extensively than the nearby Eastern Segment, is divided by the Göta Älv Shear Zone and the Dalsland Boundary Thrust into two main units; the Western and Median Segments. A garnet amphibolite located in the Median Segment, approximately 10 km east of the Göta Älv Shear Zone, was studied in order to get a better understanding of the P-T conditions of the area as well as the implications this has for the geological history of the Idefjorden Terrane. The metamorphic paragenesis and textures of the rock helped determine that the garnet amphibolite was close to equilibrium conditions during peak metamorphism and that the metamorphic minerals observed grew in the presence of partial melt. P-T calculations using the software Thermobarometry (GTB) showed that the core of the garnet grew under temperatures between 630 and 680°C and pressures between 9 and 10 kbar, while the temperature and pressure reached 680 to 750°C and 8.5 to 10 kbar during the growth of the garnet rim. The temperature intervals are consistent with observations suggesting that the rock underwent partial melting, and these P-T conditions correspond to upper amphibolite facies and a depth of between 31.5 and 37 km. Recent U-Pb data by Ingered (2019) of migmatites located close to the sample location gives a minimum age of migmatization of 1019±27 Ma in the Median Segment, which correlates well with the theory of the Idefjorden Terrane being buried to a depth of at least 35 km during the Agder phase (1.08-0.98 Ga; Bingen et al. 2008b; Ingered 2019). Evidence of local retrograde metamorphism, likely in the prehnite-pumpellyite facies, was also observed in the garnet amphibolite in the form of partial replacement of biotite by prehnite.

Keywords: P-T conditions, Sveconorwegian orogeny, Idefjorden Terrane, Median Segment, Göta Älv Shear Zone, garnet amphibolite, upper amphibolite facies, partial melting

Supervisor: Charlotte Möller

Subject: Bedrock Geology

Anna Sartell, Department of Geology, Lund University, Sölvegatan 12, SE-223 62 Lund, Sweden. E-mail: bas15asa@student.lu.se

Metamorf paragenes och P-T förhållanden i granatamfibolit från Götaälvzonen vid Lilla Edet

Anna Sartell

Sartell, A., 2019: Metamorf paragenes och P-T förhållanden i granatamfibolit från Götaälvzonen vid Lilla Edet. *Examensarbeten i geologi vid Lunds universitet*, Nr. 574, 36 sid. 15 hp.

Sammanfattning: Den Svekonorvegiska orogenesen (ca 1 Ga) ledde till rekristallisation av stora delar av sydvästra Sverige, med utbredd metamorfos och lokalt även partiell uppsmältning. Idefjordenterrängen, som har blivit studerad i mindre detalj än det närliggande Östra Segmentet, blir i söder uppdelad av Götaälvzonen i två huvudsakliga enheter; Västra Segmentet och Mediansegmentet. En granatamfibolit observerad i Mediansegmentet ungefär 10 km öster om deformationszonen studerades för att få en bättre förståelse för P-T förhållandena i området samt dess betydelse för den geologiska utvecklingen av Idefjordenterrängen. Den metamorfa paragenesen och texturerna i bergarten visade att granatamfiboliten bildades nära jämvikt under peak metamorfosen och att de metamorfa mineralen växte i närvaro av partiell smälta. P-T beräkningar med programmet Thermobarometry (GTB) visade att granatens kärna växte vid temperaturer runt 630 till 680°C och tryck mellan 9 och 10 kbar, medan temperatur och tryck nådde 680 till 750°C och 8,5 till 10 kbar då utkanten av granaten växte. Dessa temperaturintervall stämmer överens med observationer som tyder på att bergarten genomgått partiell uppsmältning och P-T förhållandena motsvarar övre amfibolitfacies samt ett djup mellan 31,5 och 37 km. Nya U-Pb dateringar av Ingered (2019) av migmatiter observerade i närheten av provtagningslokalen ger en minimiålder för partiell uppsmältning på 1019±27 Ma i Mediansegmentet, vilket sammanfaller väl med teorin att Idefjordenterrängen har blivit begraven till ett djup av åtminstone 35 km under Agderfasen (1,08-0,98 Ga; Bingen et al. 2008b; Ingered 2019). Tecken på lokal retrograd metamorfos, förmodligen i prenit-pumpellyitfacies, observerades också i granatamfiboliten i form av biotit som delvis ersatts av prenit.

Nyckelord: P-T förhållanden, Svekonorvegiska orogenesen, Idefjordenterrängen, Mediansegmentet, Götaälvzonen, granatamfibolit, övre amfibolitfacies, partiell uppsmältning

Handledare: Charlotte Möller

Ämnesinriktning: Berggrundsgeologi

Anna Sartell, Geologiska institutionen, Lunds universitet, Sölvegatan 12, 223 62 Lund, Sverige. E-post: bas15asa@student.lu.se

1 Introduction

Around 1.0 Ga, the Sveconorwegian orogeny was shaping and changing the continental crust in southwestern Scandinavia. This orogeny was significant not only in Scandinavia, but globally as a part of the assembly of the supercontinent Rodinia including the large-scale orogenic event called Grenville in Canada (Bingen et al. 2005; Bingen et al. 2008b). The resulting orogenic belt found in southwestern Sweden and southern Norway, the Sveconorwegian Orogen, can be divided into five main lithotectonic units. These are delimited by roughly N-S trending shear zones, and in some cases, similar shear zones can be found also within the units (Park et al. 1991, Bingen et al. 2008b). One such shear zone follows the river Göta Älv from Trollhättan and lake Vänern in the north to Gothenburg in the south. The shear zone then continues further south down to Kungsbacka. The Göta Älv Shear Zone marks the southern boundary dividing the lithotectonic unit Idefjorden into two separate segments, the Western and the Median Segments (Berthelsen 1980, Park et al. 1991). A limited amount of work has been done to examine and compare these two segments and how this shear zone has impacted them. A field mapping campaign covering parts of these two areas and the shear zone was therefore conducted in 2018, in collaboration with the Swedish Geological Survey and another student, Mimmi Ingered, who was writing her thesis on zircon U-Pb constraints on the timing of Sveconorwegian migmatization in the Western and Median Segments of the Idefjorden Terrane (Ingered 2019). During mapping, a locality with migmatized amphibolite bodies was found in the Median Segment and a sample was taken.

The purpose of this thesis was to examine the metamorphic paragenesis and textures of this garnet amphibolite in thin section, in order to get a better understanding of which temperatures and pressures the rock was subjected to during metamorphism and the implications this has for the Median Segment and the Idefjorden Terrane. Furthermore, possible zoning of garnets as well as the geochemical composition of various minerals was investigated, to further understand the geological history of this amphibolite. The results of this thesis will provide insight into what temperatures and pressures the Median Segment went through during Sveconorwegian metamorphism, which together with the ages obtained by Ingered (2019) will provide a significant new puzzle piece into the evolution of the Sveconorwegian orogenic belt.

2 Background

2.1 Regional Geology

2.1.1 The Sveconorwegian Orogen

The Sveconorwegian orogenic belt was formed between 1.14 and 0.90 Ga, and extends from southern Norway to southwestern Sweden (Bingen et al. 2008a; Bingen et al. 2008b). It is a continuation of the Canadian Grenville Orogen and was a part of the assembly of the supercontinent Rodinia (Bingen et al. 2005). The Sveconorwegian Orogen has been interpreted as the result of a continent-continent collision with another large continental landmass, possibly Amazonia (Bingen et al. 2005; Bingen et al. 2008b). However, this theory has been questioned by Slagstad et al. (2013; 2017) and the other explanation proposed in these articles is that the orogenic belt formed due to an accretionary orogen and underwent periods of compression and extension.

To the northwest, the orogenic belt is bounded by the Caledonides and to the east by the orogenic frontal zone, which makes up the boundary between the orogen and the Fennoscandian Foreland, and transects the Transscandinavian Igneous Belt and the Svecofennian Province. The central part of the orogenic frontal zone is made up of the Protogine Zone and the eastern part is made up of the Sveconorwegian Frontal Deformation Zone (Fig. 1; Bingen et al. 2008b; Pinán Llamas et al. 2015). The Sveconorwegian orogen is divided into different lithotectonic units, which are separated by mainly north-south striking shear zones. These are from west to east; Telemarkia, Bamble, Kongsberg, Idefjorden and Eastern Segment (Fig. 1; Bingen et al. 2008b). The two most eastern units will be described more in detail in a later chapter. The orogeny has been divided into four phases that represent the assembly of these units, the Arendal, Agder, Falkenberg and Dalene phases.

The earliest phase, Arendal, began around 1145 Ma (Engvik et al. 2016). In the Bamble and Kongsberg terranes, this time interval is characterized by high grade metamorphism. The preexisting calc-alkaline crust formed at 1650-1520 Ma, and is similar to the Telemarkia and Idefjorden terranes. Therefore, it is believed that the Bamble and Kongsberg terranes formed as tectonic wedges as a result of a collision between Telemarkia and Idefjorden (Bingen et al. 2008b). At 1080 Ma, the Agder phase began and Ingered (2019) suggests that this phase is characterized by metamorphism in the Idefjorden terrane lasting until 980 Ma. The central part of the orogen was involved in crustal thickening and imbrication, which affected the Idefjorden and Telemarkia terranes (Bingen et al. 2008b). In the Idefjorden terrane, high-pressure metamorphism reaching amphibolite- to granulite-facies occurred at the beginning of the phase, as the terrane was buried to a depth of at least 35 km (Söderlund et al. 2008; Bingen et al. 2008b). Coevally, the Telemarkia terrane was intruded by Fe-rich granitic plutons (Bingen et al. 2008b). Metamorphism in the Eastern Segment has been dated to between 1000 and 960 Ma (Möller & Andersson 2018, and references therein), suggesting that it began during the late Arendal phase and continued during the Falkenberg phase. Part of the Eastern Segment was buried to a depth of at least 60 km, which is shown by the presence of eclogites (Möller 1998; Möller et al. 2015; Tual et al. 2017). The age of eclogitisation has been dated at 988 ± 7 Ma

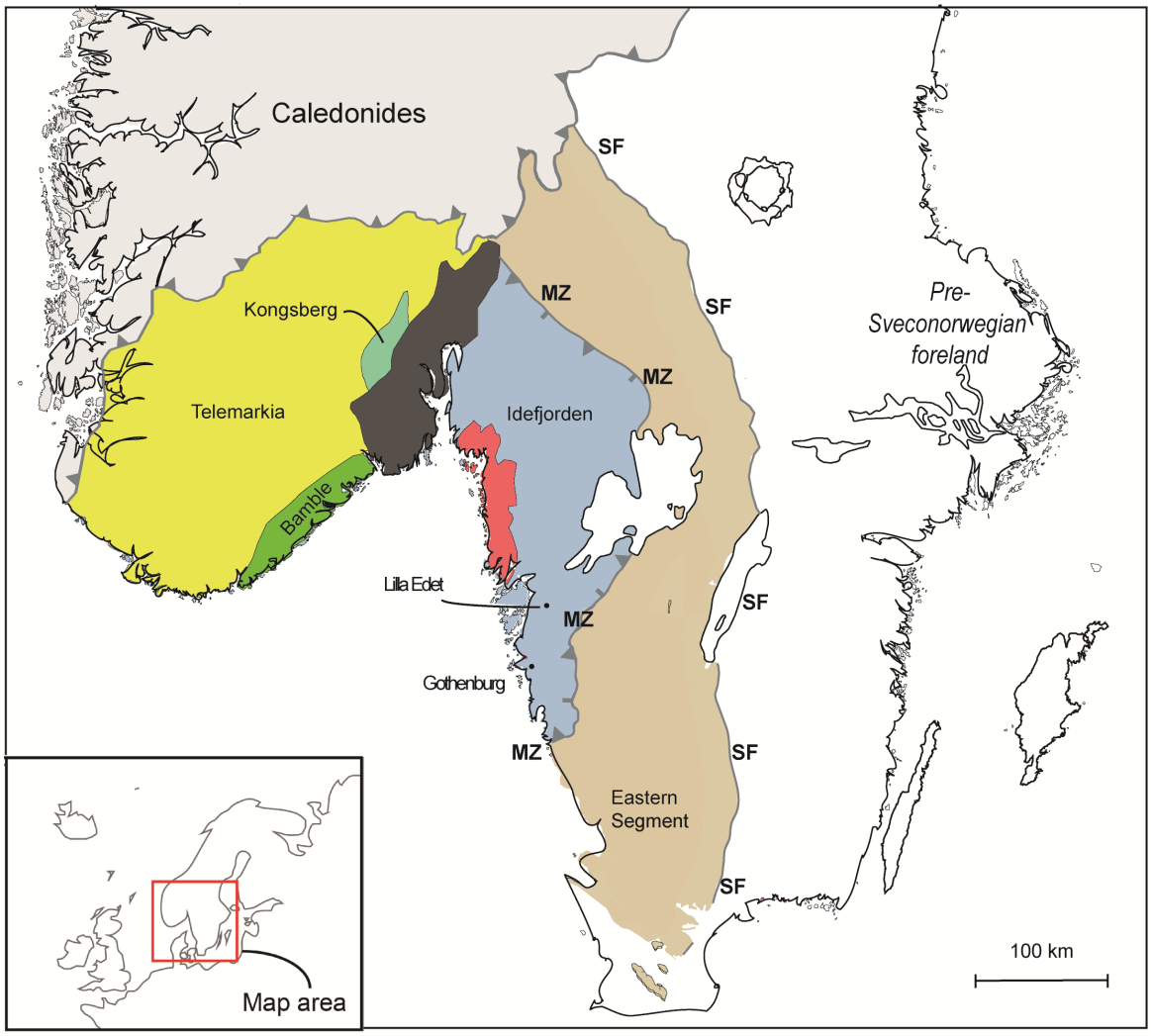

Fig. 1. Map showing the five major Sveconorwegian lithotectonic units as well as major shear zones. The Bohus Granite is marked in red. Gothenburg and Lilla Edet, which is located approximately 10 km west of the sample location, are also marked out. MZ = the Mylonite Zone, SF = Sveconorwegian Frontal Deformation Zone. Modified from Pinán Llamas (2015).

(Möller et al. 2015; see also Johansson et al., 2001). The formation of eclogites was shortly followed by their partial exhumation to depths of c. 40 km, at 980-970 Ma (Möller 1998, 1999; Möller et al. 2015, Tual et al. 2017, 2018), and concomitant high-grade metamorphism of the Eastern Segment. There is also evidence of amphibolite-facies metamorphism and migmatization along two of the major shear zones found in western Sweden, the Mylonite Zone and the Göta Älv Shear Zone, around 980-970 Ma (Andersson et al. 2002; Ahlin et al. 2006). The last phase, Dalene (960-900 Ma), is interpreted as extension and relaxation as the orogen collapsed. In both the Telemarkia and Idefjorden Terranes, post-collisional magmatism is associated with this extension (Bingen et al. 2008b).

2.1.2 Idefjorden Terrane

The Idefjorden terrane is mostly located in western Sweden and has been interpreted as allochthonous. It lies west of and structurally above the Eastern Segment, with the roughly N-S trending Mylonite Zone defining a border between the two (Fig. 1; Bingen et al. 2008b). The terrane consists of both volcanic and plutonic calc-alkaline and tholeitic rocks, which formed during the Gothian accretionary event between 1.65 and 1.52 Ga (Bingen et al. 2008b). The Idefjorden Terrane has previously been divided into the Median Segment and the Western Segment by Berthelsen (1980), and this division has been used by other authors as well (Park et al. 1991). These two segments are separated by the Dalsland Boundary Thrust north of Lake Vänern and the Göta Älv Shear Zone in the south (Fig. 2; Park et al. 1991).

The Median Segment is made up of the Göteborg-Åmål Suite, the Horred Formation as well as the Dal Formation (Fig. 2). The Göteborg-Åmål Suite consists of volcanic, plutonic and sedimentary rocks formed in a continental volcanic arc around 1.63-1.59 Ga (Bingen et al. 2008b; Åhäll & Connelly 2008). The older metavolcanic Horred Formation formed at 1.65 Ga, whereas the 1.1 Ga Dal Formation consists of early Sveconorwegian volcanic and sedimentary rocks (Brewer et al. 2002; Åhäll & Connelly 2008). The

Western Segment contains the Hisingen Suite, the Stora Le-Marstrand (SLM) Formation and the Bohus Granite (Fig. 2; Bingen et al 2008b; Åhäll & Connelly 2008). The Hisingen Suite consists of granitic rocks which intruded around 1.58-1.52 Ga, and the SLM, which formed at the same time around 1.59-1.55 Ga, is made up of metasedimentary graywackes with widespread metabasalts, exhibiting a varying degree of migmatization (Åhäll & Connelly 2008). The Bohus Granite intruded the SLM formation post-kinematically at 0.92 Ga (Eliasson & Schöberg 1991). The Kungsbacka Bimodal Suite can be found in both the Median and Western Segment, and it forms a belt of 1.34-1.30 Ga granitic plutons which follows the Göta Älv Zone and the Dalsland Boundary Thrust (Hegardt et al. 2007).

The Sveconorwegian metamorphism in the Idefjorden Terrane occurred during the Agder phase, between 1.08 and 0.98 Ga (Ingered 2019). The metamorphic grade varies, mainly ranging from greenschist to amphibolite facies, but also locally reaching high-pressure granulite facies in mafic boudins east of the Göta Älv Shear Zone (Söderlund et al. 2008). Indirect estimates for extension along the Mylonite Zone are set around 910-920 Ma (Bingen et al. 2008b). The Sveconorwegian structural grain found in the Idefjorden Terrane is generally N-S to NW-SE, same as the orogen-parallel shear zones found within the terrane (Bingen et al. 2008b). Examples of such orogen-parallel shear zones are both the aforementioned Dalsland Boundary Zone and the Göta Älv Shear Zone, but also the Ørje Shear Zone, which is found in the Idefjorden Terrane in south-eastern Norway. These have been interpreted as transpressive thrust zones (Park et al. 1991).

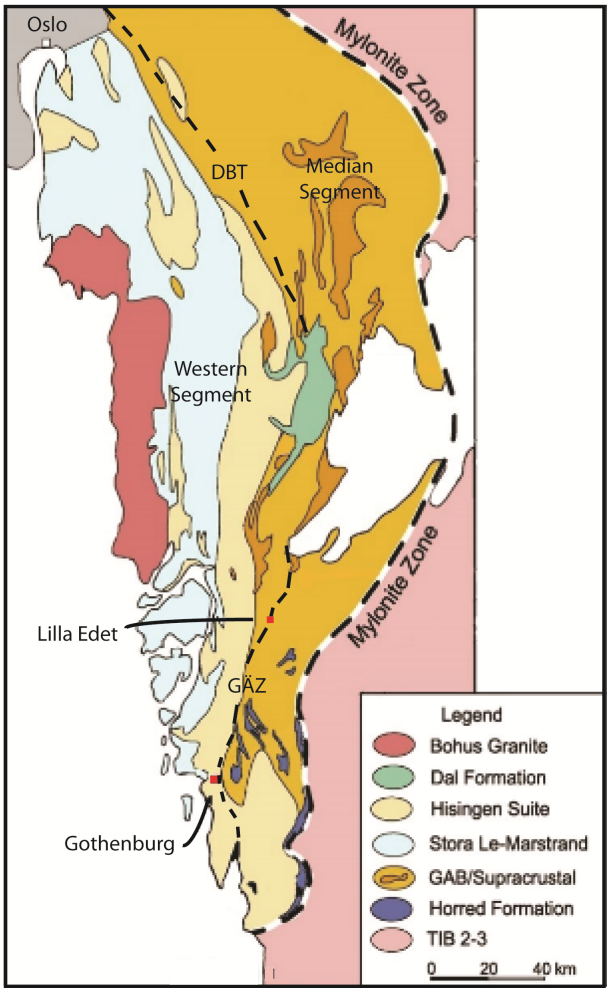

Fig. 2. Map over the main units found in the Idefjorden Terrane. The Göta Älv Shear Zone (GÄZ) and the Dalsland Boundary Thrust (DBT) divides the terrane into the Western and Median Segments. Modified after Ingered (2017) and Åhäll & Connelly (2008).

2.1.3 Eastern Segment

The Eastern Segment is the easternmost unit affected by the Sveconorwegian orogeny. It is interpreted as parautochthonous and has been lithologically correlated to the Transcandinavian Igneous Belt, which is the foreland found on the Fennoscandian side of the orogen (Bingen et al 2008b). The Eastern Segment, unlike the other main units of the Sveconorwegian orogen, is Paleoproterozoic. It consists of 1.80-1.64 Ga granitoids, which has been overprinted by Hallandian amphibolite-facies metamorphism at 1.46-1.41 Ga and later also Sveconorwegian metamorphism (Möller et al. 2007, 2015; Bingen et al. 2008b; Beckman et al., 2017; Möller & Andersson 2018). Its eastern boundary is made up of the Sveconorwegian Frontal Deformation Zone and the Protogine Zone, and to the west the Eastern Segment borders the Idefjorden Terrane by the west-dipping Mylonite Zone (Andersson et al. 2002; Bingen et al. 2008). Sveconorwegian metamorphism affected the Eastern Segment during 0.99-0.96 Ga and the metamorphic grade reached upper amphibolite- to high-pressure granulite-facies. Remnants of eclogite are present in a tectonic unit just below the Mylonite Zone, in the Eastern Segment (Möller 1998; Möller et al., 2015; Tual et al., 2015, 2017). The general trend of the segment is an increase of Sveconorwegian metamorphism from east to west and from north to south (Bingen et al. 2008b; Möller & Andersson, 2018).

2.2 Field description of the area

The bedrock of the Western and Median Segments of the Idefjorden Terrane were mapped during an internship with the Swedish Geological Survey in 2018, in collaboration with MSc-student Mimmi Ingered. The area of interest is located near Lilla Edet, a small city located by the Göta Älv river approximately 50 km north of Gothenburg (Fig. 1; Fig. 2; Fig. 3). The Göta Älv Shear Zone runs parallel to the river and is continued north of lake Vänern by the Dalsland Boundary Thrust, but Park et al. (1991) found that there is not just two major shear zone dividing the Median and Western Segments. Instead, they noted the presence of an intricate network of branching shear zones, especially in the north. It is not known if the Göta Älv Shear Zone in the Lilla Edet area is one uniform zone or rat-

her a system of several shear zones (Park et al. 1991). However, observations made by the author and Ingered in 2018 suggests that the Göta Älv Shear Zone in the Lilla Edet area appears as one or several shear zones located in close proximity, covering an area with a width of around 1-2 km and a NE-SW trend. The general dip is 40° with a dip direction towards the NW (Park et al. 1991). According to unpublished data collected by the author and Ingered in 2018, the shear zone is characterized by brittle deformation, which seems to postdate earlier ductile deformation of the area. Elongation lineations found in the southern region of the Göta Älv Shear Zone generally plunges 30° NW (Park et al. 1991). Shear bands and augen tails indicates that there has been both normal and reverse movement (Park et al. 1991). Some observations by Park et al. (1991) suggests that the normal-sense movements occurred later than the thrust sense, which is to be expected as a collision is followed by post-collisional extension.

The purpose of the 2018 field campaign was to compare the two segments and how the bedrock varied depending on the proximity to the shear zone. Granitic to granodioritic gneisses are common in both segments, but shows a greater degree of migmatization in the Median Segment. Augen varieties can be found in both segments. Pegmatite bodies and dikes have intruded both sides of the Göta Älv Shear Zone; these are rarely deformed in the Western Segment but are almost always deformed in the Median Segment. Ductile deformation can be observed in both segments, with brittle deformation being more common closer to the shear zone. Near the Göta Älv Shear Zone, quartz-filled fractures can be found in the Median Segment, and slickensides and faults are abundant on both sides. In the Western Segment, smaller mafic lenses of amphibolite can be observed, but no larger mafic bodies. Garnet has not been observed in this segment, neither in gneisses or mafic lenses. The Median Segment contains both smaller mafic lenses, mafic dikes, larger amphibolite bodies as well as ultramafic rocks. Both gneisses and amphibolites are commonly garnet-bearing. The ultramafic rocks can be found as a N-S trending band of bodies appearing as hills in the landscape, each meter to tens of meters in size. The mafic lenses and dikes consist of amphibolite, and the latter are folded together with migmatites near the sample location. The dominant strike direction in the area is N-S to NE-SW, with an easterly to south-easterly dip direction and dip values varying from 10 to 60° in the Median Segment and from 20 to 80° in the Western Segment.

The sample was taken in the Median Segment, approximately 10 km east of the Göta Älv Shear Zone. Several migmatized garnet amphibolite bodies dipping towards the north-west can be observed at a railroad locality near Hälltorp (cover photo). The migmatization observed in the amphibolite were classified according to Mehnert (1968; see also Sawyer 2002) and the following kinds were found: net-like structures, dilation structures, schlieren structures and agmatitic migmatites. Surrounding the garnet amphibolite bodies is a lighter colored, stromatic migmatite consisting mostly of plagioclase, biotite, hornblende and garnet. The amphibolite sampled at the locality north of Hälltorp can be found on the western side of the railroad and has large garnet porphyroblasts with rims of plagioclase and possibly quartz (Fig. 5).

2.3 Garnet amphibolites

2.3.1 General description

According to Hibbard (1995), the name “amphibolite”

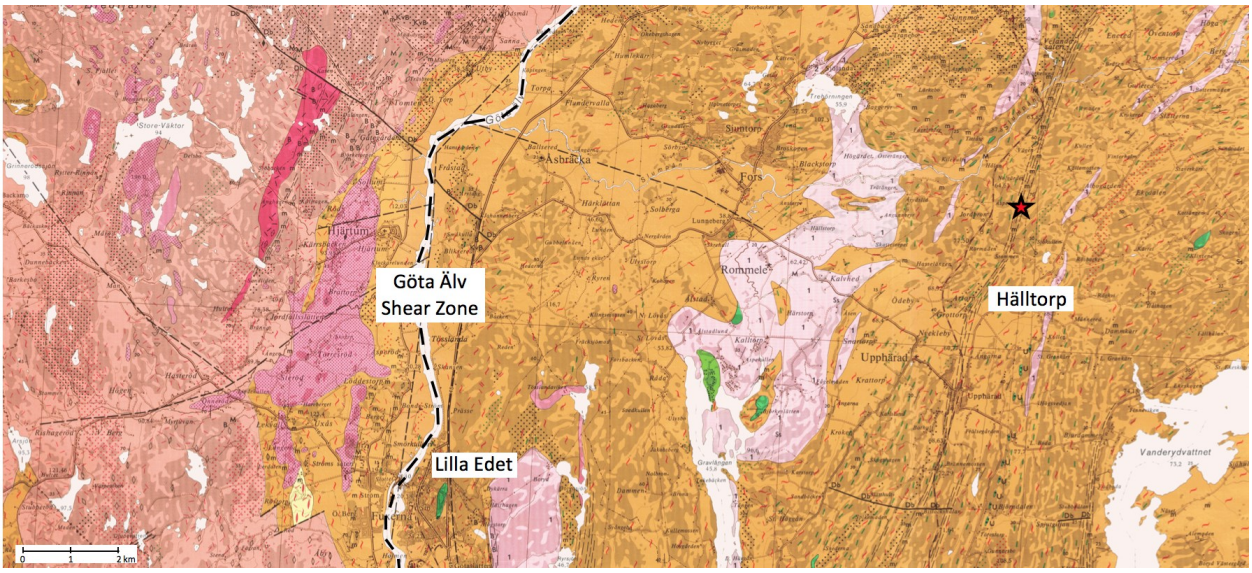

Fig. 3. Map showing the bedrock geology of the area, from the Swedish Geological Survey. Lilla Edet and Hälltorp are marked out, as well as the approximate location of the Göta Älv Shear Zone along the Göta Älv river. The sample location is marked with a red star. Legend for the map can be found in Appendix I. Modified after Samuelsson & Lundqvist (1988); Ingered (2019).

merely indicates a relatively coarse rock consisting of plagioclase and amphibole. Best (1982) goes further to say that an amphibolite is composed mainly of hornblende and plagioclase, but with minor amounts of biotite, sphene, quartz, pyroxene and almandine-rich garnets being possible. It is also mentioned that the anorthite percentage found in the plagioclase typically places it in the oligoclase to andesine range and that hornblendes tend to be of the sodic aluminous variety (Best 1982).

2.3.2 Idefjorden Terrane

Very few garnet amphibolites within the Idefjorden Terrane have been studied in detail. However, pressure -temperature (P-T) calculations have been made in the Stora Le-Marstrand Formation in the Koster archipelago (Gunnarsson & Forsström 2012). This area of the Western Segment was intruded by c. 700 diabase dikes around 1450 Ma, and Gunnarsson & Forsström (2012) calculated the Sveconorwegian temperatures of a garnet poor diabase as well as the reaction zone between a diabase and the surrounding bedrock to around 650-690°. Furthermore, the P-T conditions and geochronology of two metamorphosed diabase dikes located 5 km east of the Göta Älv Shear Zone in the Median Segment have been studied by Söderlund et al. (2008). These two dikes are located approximately 10 km north of our sample location, Hälltorp. The Lunden dike was found to have recrystallized during metamorphism at around 15 kbar and 740°C, which corresponds to granulite facies. The upper age limit of metamorphism was found to be 1046±6 Ma. The second dike studied, the Haregården dike, was recrystallized in upper amphibolite to granulite facies, with pressures reaching c. 10 kbar and 700°C. The transition between igneous and metamorphic mineralogies has been placed at 1026±4 Ma (Söderlund et al. 2008).

2.3.3 Eastern Segment

There is a larger number of studies of garnet amphibolite bodies within the Eastern Segment. According to Söderlund (1999), Sveconorwegian metamorphism in the Åker metabasite, which is a strongly deformed garnet amphibolite found west of the Protogine Zone, reached 10-12 kbar and 600-630°C. This metamorphism has been dated to 1006±68 Ma (Söderlund et al. 2004). This metabasite is one of several found along the Protogine Zone and in the Eastern Segment. Another example is the Herrestad garnet amphibolite. This metabasite reached temperatures around 610±40°C and pressures around 9±0.5 kbar, at 970±7 Ma (Karlstedt 2017; Beckman et al. 2017).

3 Methods

3.1. Previous sampling and preparation

The sample was taken in April 2018 in the Median Segment (Fig. 3). In January 2019, three rock chips were cut in preparation for thin section production and in March, the three thin sections were received from the manufacturer. They are named AMS18-8-1A, AMS18-8-1B and AMS18-8-1C, but will be referred to as A, B and C respectively. 8-1A was the name of the locality sampled.

3.2. Polarization microscopy

All three thin sections were examined in both plane polarized light (PPL) and crossed polarized light (XPL) using a polarization microscope of the model Olympus BX53F2. The main focus was to determine the main mineral assemblage and to describe the textures present in the rock. Unknown minerals and specific minerals of interest were noted on scanned photographs of the thin sections, to be able to observe them in more detail during scanning electron microscopy. Photographs at different magnifications were taken of the thin sections using a camera connected to the Olympus microscope. When describing minerals, the abbreviations listed in Whitney and Evans (2010) are used.

3.3. Scanning electron microscope – Energy Dispersive X-ray Spectroscopy (SEM-EDS)

Thin section A was chosen for further examination using a scanning electron microscope coupled with energy dispersive X-ray spectroscopy (EDS-SEM) (Fig. 4). This thin section was chosen since it was deemed to be a good representation of the sample as a whole, as it contains one garnet porphyroblast as well as some domains where quartz and plagioclase are the dominant minerals. The analysis was made at the Department of Geology at Lund University, using a SEM of the model Tescan Mira3 together with the Oxford EDS system. The primary current used was 147 mA, the accelerating voltage was 15 kV and the total analysis time was approximately 30 s. The analyses were calibrated using a cobalt standard and the software Aztec was used for further analysis of the data gathered.

Elemental analysis was done to examine if zoning was present in the garnets and to determine the chemical composition of various minerals. Three micro domains were set up within different areas of the garnet, two by the edge and one near the center (Fig. 4). Within each of these domains, hornblende, plagioclase and garnet was analyzed. Several points in each mineral type were analyzed in order to ensure a stable signal and a representative composition. One analysis from each of the three minerals in each domain was chosen for pressure temperature calculations (P-T calculations) using the software GTB. These points were chosen based on which analysis had the most correct stoichiometric proportions. Two geothermometers based on hornblende and garnet were used, Graham and Powell (1984) and Perchuk et al. (1985). For the barometric calculations, the six geobarometers by Kohn and Spear (1989; 1990) were used, which are based on coexisting plagioclase, hornblende, garnet and quartz.

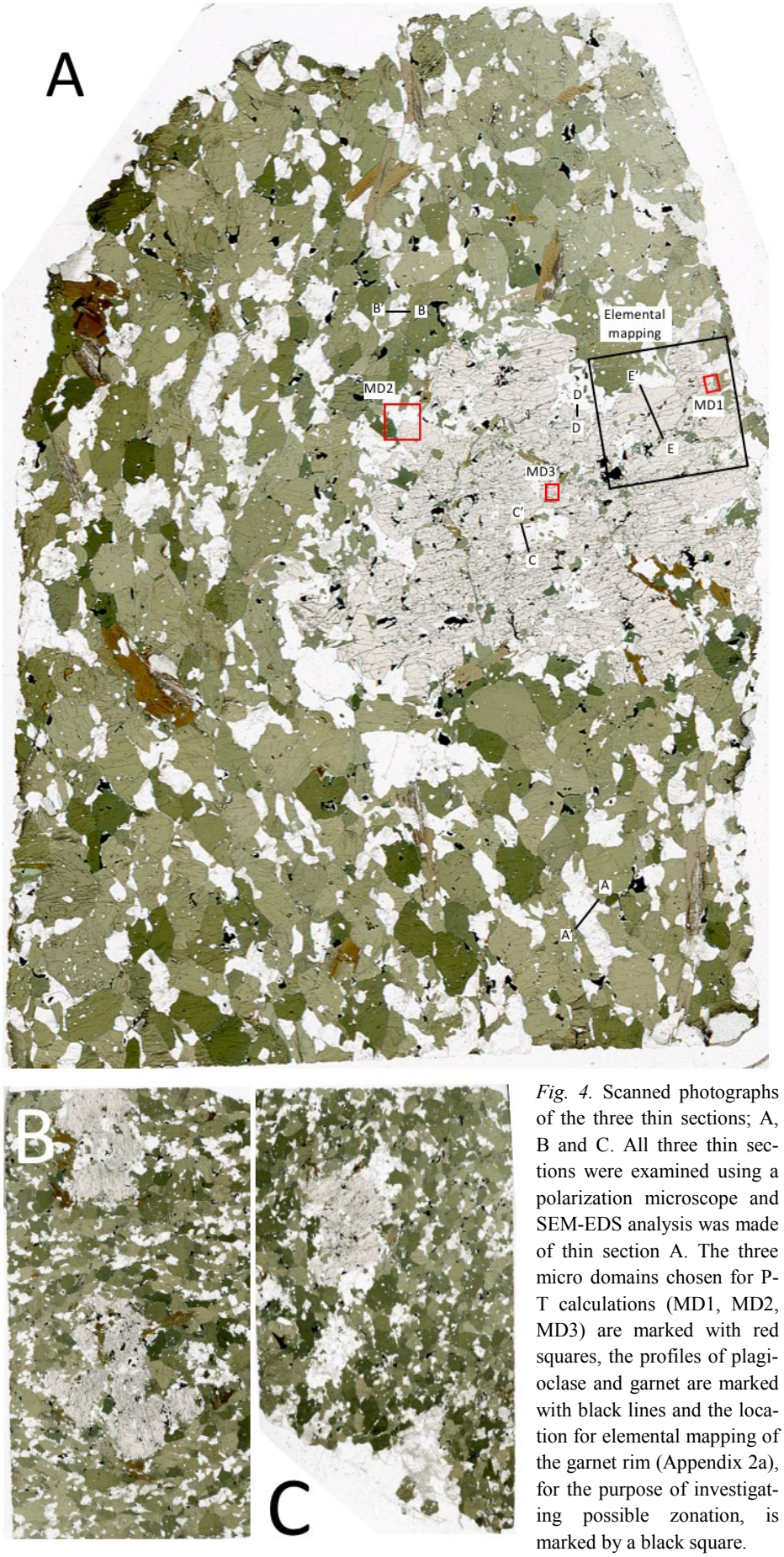

Fig. 4. Scanned photographs of the three thin sections; A, B and C. All three thin sections were examined using a polarization microscope and SEM-EDS analysis was made of thin section A. The three micro domains chosen for P-T calculations (MD1, MD2, MD3) are marked with red squares, the profiles of plagioclase and garnet are marked with black lines and the location for elemental mapping of the garnet rim (Appendix 2a), for the purpose of investigating possible zonation, is marked by a black square.

Profiles of elemental composition were made of one section of a large garnet porphyroblast as well as four plagioclase grains. For both the profiles and the analyses within the micro domains, the relative amounts of the different garnet end-members were calculated as well as the percentage of anorthite and albite components in plagioclase. To further look for zonation in garnet, elemental mapping of three areas were made. Amphiboles were classified using the method presented in Leake et al. (1997). EDS analysis was also used to identify some minerals observed in thin section where identification was not possible using only a polarization microscope. The volumes of Deer, Zussman and Howie (1962; 1982; 2001) of rock-forming minerals were used to aid in this identification. The general equation presented in Droop (1987) was used to determine if ferric iron (3+) was present. The names of minerals have been abbreviated according to Whitney & Evans (2010).

4 Results

4.1 Observations in hand sample

The two main minerals observed in hand sample were amphiboles and garnet porphyroblasts (Fig. 5). Some regions of light colored minerals were observed, both in the matrix and as rims surrounding the garnets. These lighter colored minerals were thought to be plagioclase as well as possibly some quartz.

Fig. 5. Photo of the garnet amphibolite in hand sample. The lighter colored minerals were found as tails such as is shown in this photo, but also as rims surrounding the garnets and as smaller separate domains.

4.2 Observations with polarization microscope

Polarization microscopy confirmed that the two most dominant minerals in the sample were amphiboles and porphyroblasts consisting of garnet.

4.2.1 Thin section A

This thin section contains one garnet porphyroblast with numerous inclusions. The inclusions occur as single crystals, as composite inclusions and in fractures. The garnet appears more fractured and inclusion rich towards its center. The inclusions consist of amphibole, plagioclase, quartz, biotite and opaque minerals, i.e. the same minerals which forms the matrix. Some of the amphibole crystals in the composite inclusions appear euhedral.

The most abundant mineral in the matrix is hornblende. These grains are evenly sized, often have sharp grain contacts with triple junctions and a well-developed cleavage. The largest biotite grains in the matrix show signs of alteration, with another mineral appearing to have grown along the biotite crystals' cleavage planes, and the biotite has deformed and bulged out in the areas with the most alteration. In PPL, this mineral is colorless and in XPL it presents with moderate to high interference colors, from pink to blue. It was suspected to be either pumpellyite or prehnite, but microprobe analysis was needed in order to make a confident identification. The biotite grains showing signs of this type of alteration are found together with hornblende, quartz and plagioclase with sericite/sausserite alteration. In one case, a zircon grain was also found together with the altered biotite. Plagioclase and quartz are commonly intergrown, in the matrix, along the rims of the garnet porphyroblasts, as well as inside the garnet as inclusions. The plagioclase often exhibits albite twinning. A mineral thought to be either rutile or titanite is also found in the thin section, almost exclusively in amphibole together with an opaque mineral. The amphibole grains have a varying degree of micro fractures along their cleavage planes. Some amphibole grains also have small inclusions, which appear to be plagioclase or quartz.

4.2.2 Thin section B

The second thin section is similar to thin section A, but has two slightly smaller garnet porphyroblasts. Several of the amphibole grains in the matrix exhibit sharp contacts and triple junctions are common. Simple twinning was observed in amphiboles and albite twinning in plagioclase. The mineral suspected to be rutile or titanite is found together with opaque minerals, often in amphibole. In one case, the opaque mineral was found to be completely encased in rutile/titanite. Zircon is also found in the thin section A, both in amphibole and between grains. The inclusions in garnet are smaller than in thin section, and they are located closely together. There are a lot of fractures in the garnet with small inclusions. A part of the plagioclase grains

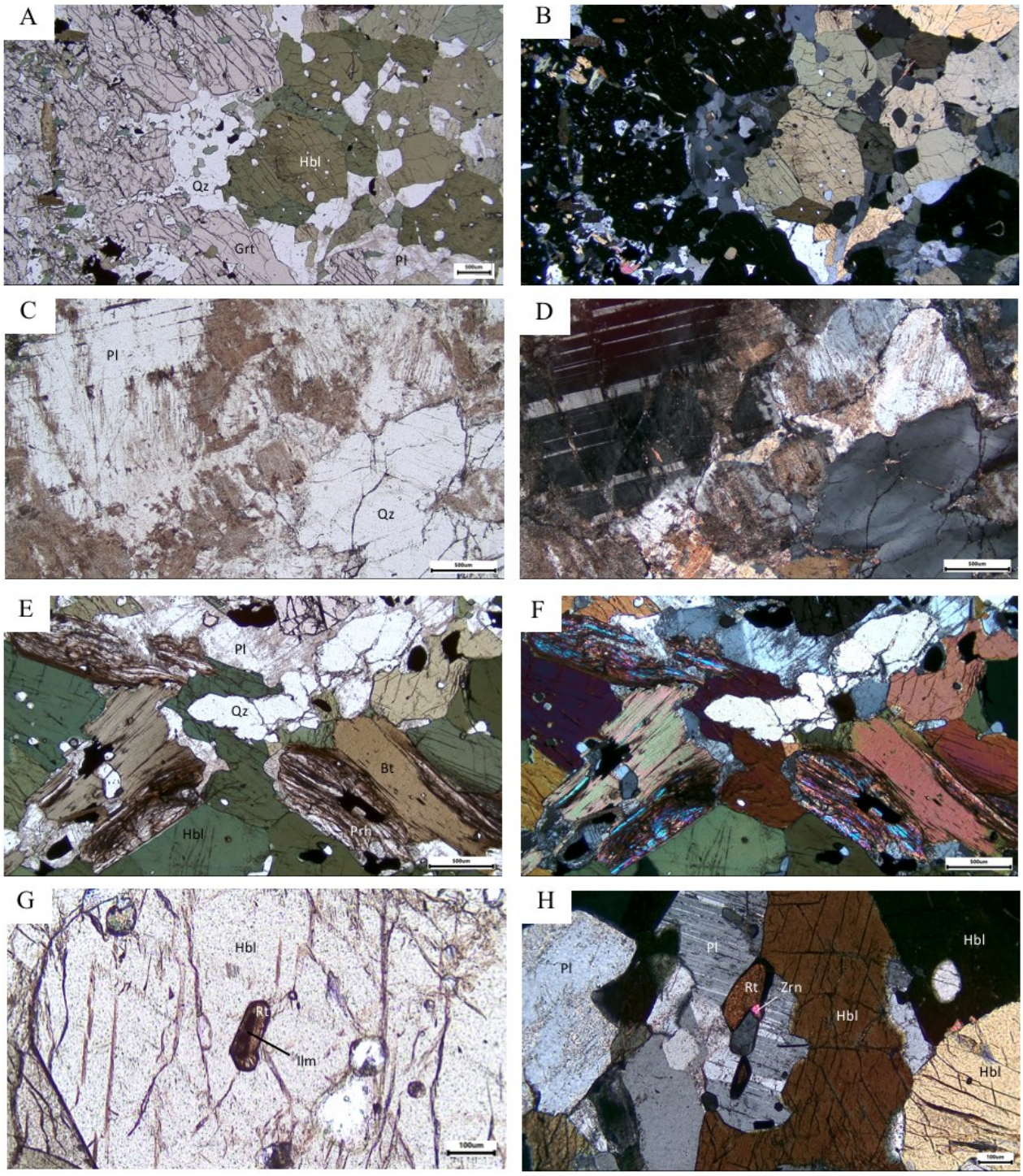

Fig. 6. Photomicrographs of garnet amphibolite from Lilla Edet. A. The edge of the garnet porphyroblast in thin section A (plane light, PPL). B. Same as A, but with crossed polars (XPL). C. Quartz and plagioclase rich domain in thin section C (PPL). Albite twinning and sericitization can be observed in the plagioclase grains and the quartz is easily recognized by its "clean" appearance. D. Same as B, but in XPL. E. Biotite crystals with partial replacement by a colourless mineral (PPL, thin section C). Surrounding minerals include amphiboles, quartz and partly sericitized plagioclase. F. Same as E, but in XPL. G. Rutile grain with ilmenite core, located inside a larger amphibole grain (thin section B, PPL). H. Two rutile grains in plagioclase near amphibole, in thin section B (XPL). A zircon grain, identified though its high relief and high-order interference colors. The characteristic cleavage of amphibole can be observed in this photo as well as albite twinning and some sericitization in plagioclase.

has undergone sericitization/saussuritization. The matrix is similar to that in thin section A, but small amounts of chlorite is also found in the matrix.

4.2.3 Thin section C

The third thin section has one garnet porphyroblast, similarly to thin section A. It also has two larger domains where sericite/sausserite altered plagioclase and quartz are the dominant minerals instead of amphibole, which is dominant in the rest of the matrix. This is a difference from the other two thin sections. These two minerals can also be found along the rim of the garnet and between amphiboles in the grain contacts. Small amounts of chlorite are also present in the matrix, like in thin section B. Zircon is an accessory mineral just as in the other thin sections.

4.3 Observations with SEM-EDS

4.3.1 Elemental mapping

Elemental mapping of the garnet porphyroblasts in thin section A showed that no chemical zoning was present (Appendix II.a, b and c). Three domains were mapped, one at the rim of the garnet and two close to the core. The first domain showed that there is a rim of plagioclase along most of the edge of the garnet. The amount of Fe in the garnet is uniform over the surface mapped. Some areas have a higher concentration, and these are opaque minerals (cp. BSE image). Also Mg is uniform within the garnet, with the areas with higher Mg amounts representing amphibole grains in fractures or inclusions. Garnet is the mineral which shows the highest concentration of Mn, and no zonation is visible. Ca is low in both garnet and plagioclase. The Si map shows clearly where quartz is located in the matrix and as inclusions within the garnet.

The second area mapped, close to the core of the garnet, shows that the Al amounts in plagioclase and garnet are closer to each other than near the edge of the garnet. The Ca amount is low for both plagioclase and garnet, just as in area A. The Fe amount does not vary substantially within the garnet, and neither does Mg or Mn.

The last area mapped shows that Al is evenly distributed across the garnet. The plagioclase has a bit more Al than the garnet. Ca is once again not detected in large amounts. Also in the Fe, Mg and Mn maps, no particular zonation of garnets is visible.

Table 1. Data from microprobe analysis of thin section A. The data presented was used for P-T calculations, Pl + Hbl + Grt for geobarometry and Hbl + Grt for geothermometry. The data has not been corrected for Fe (3+). (Pl=plagioclase, Hbl=hornblende, Grt=garnet).

	Micro domain 1			Micro domain 2			Micro domain 3		
	Pl	Hbl	Grt	Pl	Hbl	Grt	Pl	Hbl	Grt
SiO_2	58.5	41.09	37.61	59.43	42.15	37.39	59.17	41.95	37.68
TiO_2		1.39			1.12			1.35	
Al_2O_3	25.81	14.31	21.12	25.34	13.12	21.33	25.4	13.79	21.5
MgO		9.15	4.42		9.55	4.58		10.72	4.62
FeO	0.13	16.92	25.8	0.12	17.3	25.26	0.37	14.88	25.08
MnO		0.25	2.78		0.24	2.42		0.19	2.14
CaO	7.22	11.1	7.57	6.59	11.14	7.61	6.72	11.09	7.71
Na_2O	7.34	1.69		7.71	1.66		7.61	1.72	
K_2O		0.86		0	0.78			1.07	
Total	99.01	96.76	99.3	99.2	97.06	98.6	99.28	96.75	98.73
Si	2.64	6.23	2.99	2.67	6.37	2.98	2.66	6.3	2.99
Ti		0.16			0.13			0.15	
Al	1.37	2.56	1.98	1.34	2.34	2	1.34	2.44	2.01
Mg		2.07	0.52		2.15	0.54		2.4	0.55
Fe	0.01	2.15	1.71	0	2.19	1.68	0.01	1.87	1.66
Mn		0.03	0.19		0.03	0.16		0.02	0.14
Ca	0.35	1.8	0.64	0.32	1.8	0.65	0.32	1.79	0.66
Na	0.64	0.5		0.67	0.49		0.66	0.5	
K	0	0.17		0	0.15		0	0.2	
Cation sum	5	15.66	8.03	5	15.65	8.02	5	15.68	8.01
Oxygen	8	23	12	8	23	12	8	23	12

4.3.2 Analysis of micro domains

In each of the micro domains, several analysis points were made of garnet, hornblende and plagioclase. For pressure and temperature calculations, one analysis of each mineral was selected for each micro domain and these are presented in Table 1. A table over the complete data set can be found in Appendix III, IV and V. SEM images of the three micro domains can be seen in Appendix VI. The anorthite and albite percentages were calculated for all plagioclase analyses in each micro domain using the formula An = Ca/(Ca+Na+K). The results show that the majority of plagioclase is andesine, with a few oligoclase (Fig. 7; Deer et al. 2001). The anorthite content varies from 29 to 38 mole-%. Based on the amounts of Fe, Mg, Mn and Ca in garnet in the three domains, the mole-fractions of the garnet species grossular ($Ca_3Al_2Si_3O_{12}$), spessartine ($Mn_3Al_2Si_3O_{12}$), pyrope ($Mg_3Al_2Si_3O_{12}$) and almandine ($Fe_3Al_2Si_3O_{12}$) were calculated (Fig. 8). Almandine is most abundant, with contents varying from 55 to 56 %. Grossular was the second most common, being 21 to 22 % of the garnet. Spessartine made up 5 to 7 % of the garnet and the pyrope component was 16 to 19 % (Figure 8). The amphiboles analyzed with SEM-EDS were classified using Leake et al. (1997), and in all three micro domains amphibole was found have a composition spanning between edenite ($NaCa_2(Mg,Fe^{2+},Mn)_5Si_7AlO_{22}(OH,O,F,Cl)_2$) and pargasite or magnesiohastingsite ($NaCa_2((Mg,Fe^{2+},Mn)_4(^{VI}Al,Fe^{3+}))Si_6Al_2O_{22}(OH,O,F,Cl)_2$), most analyses falling in the latter field.

4.3.3 Profiles

The profiles made across four plagioclase grains in different locations in thin section A show slight variations in composition (Fig. 9). However, similar to the spot analyses of plagioclase shown in Fig. 7, most analyses plot around the oligoclase-andesine border. Profiles A and B were made through plagioclase grains found in the matrix, C is a profile of plagioclase in a composite inclusion in garnet, and D is a profile of plagioclase that forms a rim around the garnet. The location of these profiles can be found in Figure 4 and electron images of the areas analyzed can be found in Appendix VII. In profile A, there is one point which does not follow the general trend. This was not removed, as the stoichiometry of this point was deemed to be correct for plagioclase. The examination of whether the stoichiometry was correct was made by comparing the number of ions found during analysis to the number of ions expected by the chemical formula for the mineral. Furthermore, in profile B, which is a plagi-

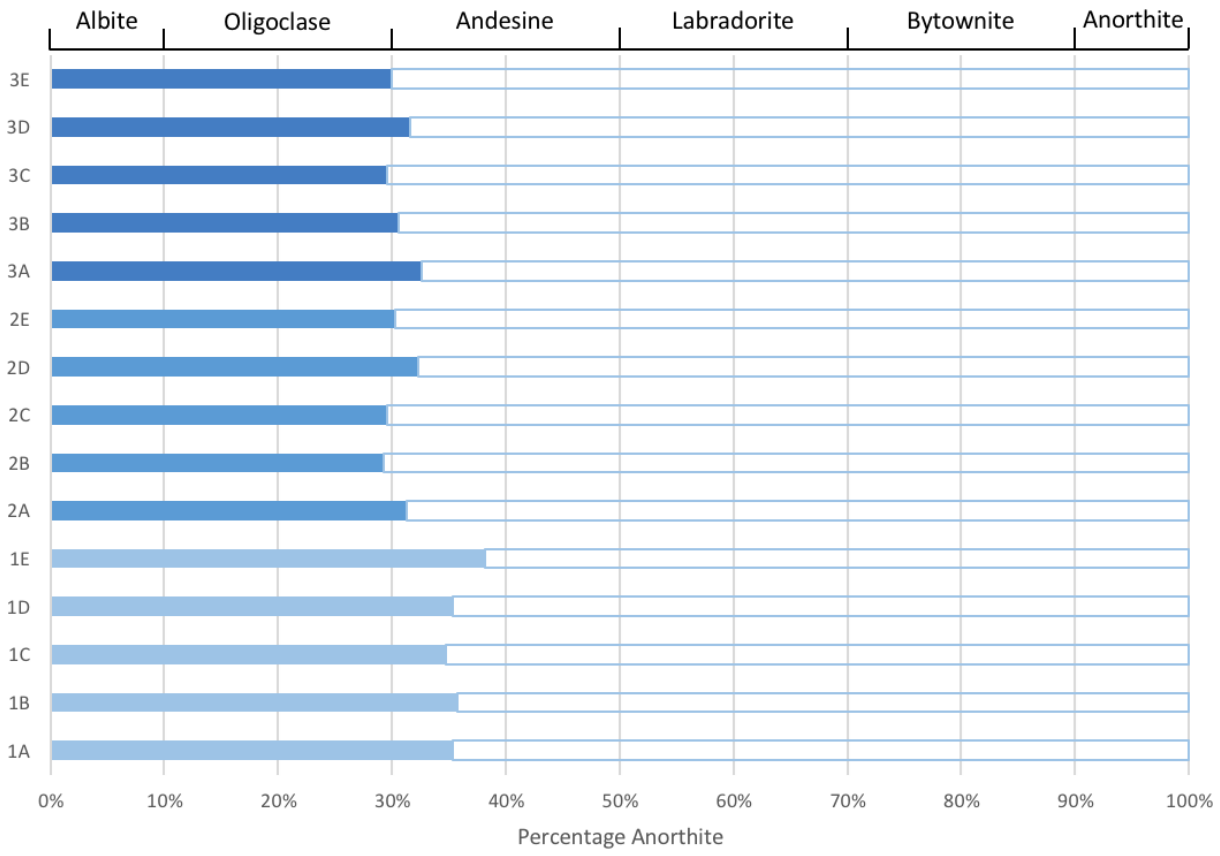

Fig. 7. Stacked bar chart showing the composition of plagioclase (spot analyses) in the three domains used for thermobarometry. The numbers 1-3 on the left refer to micro-domains and A-E mark the specific analysis points. Plagioclase classification is based on the anorthite content (Deer et al 2001, Klein & Philpotts 2013). Analyses classify as andesine or oligoclase, with the majority in the andesine field.

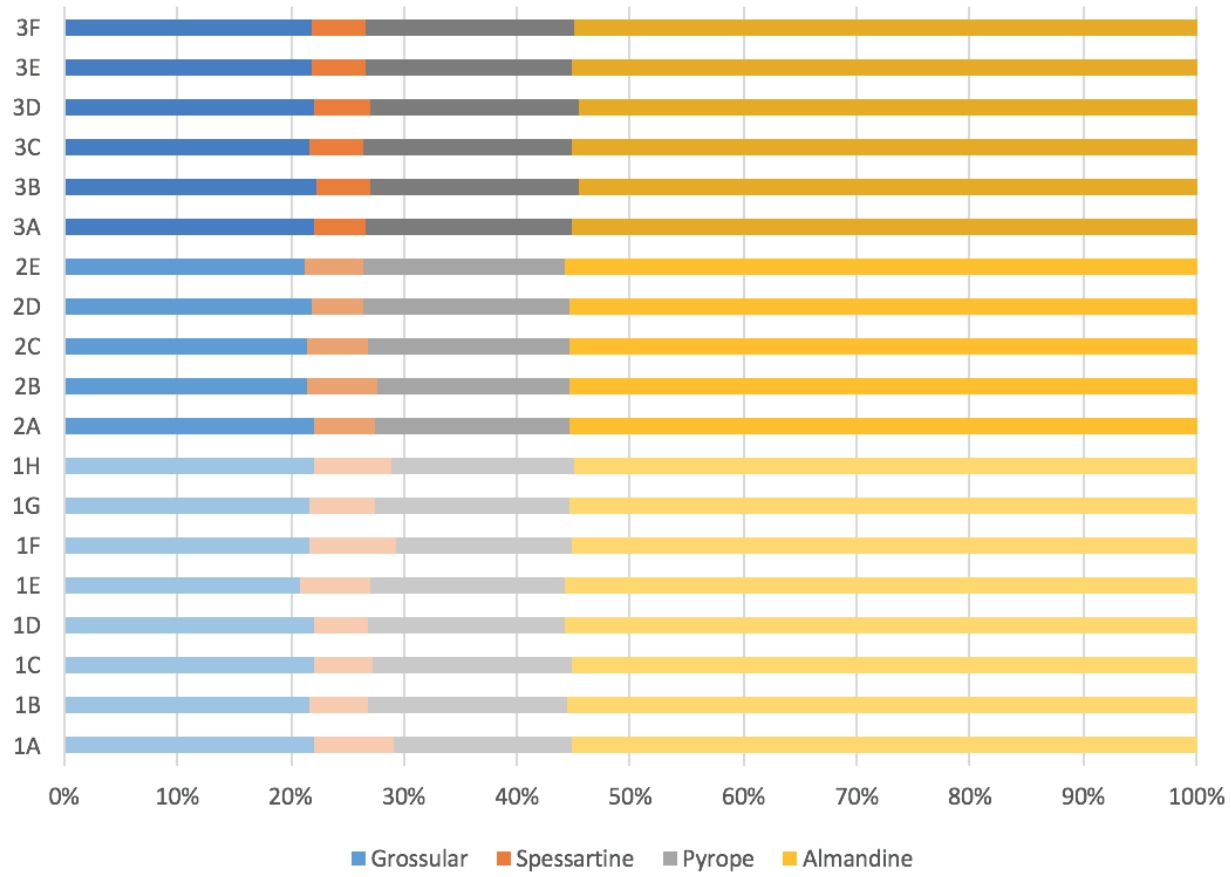

Fig. 8. Stacked bar chart showing the composition of garnet (spot analyses) in the three micro domains. Numbers 1-3 (left) refer to micro-domain and A-E to the specific analysis point. The garnet species andradite containing Fe(3+) was not included in chart as Fe (3+) was assumed to not be present, after calculations based on Droop (1987).

oclase grain in the matrix, the anorthite content decreases drastically by B'. These analyses are also stoichiometrically correct.

One profile was also made of the garnet porphyroblast found in thin section A (Fig. 10). This was taken at the rim of the porphyroblast, as can be seen in Figure 4. An electron image of the area analyzed can be found in Appendix 7. Almandine is most abundant and makes up 52 to 57 % of the garnet. The garnet consists of 21 to 25 % grossular, 15 to 20 % pyrope and 4 to 6 % spessartine (Fig. 10).

4.3.4 Identification of unknown minerals

The mineral which appeared to have formed through replacement of biotite, was identified as prehnite by comparing the data from EDS analysis to Deer et al. (1982; Table 2). All analysis points within the two grains analyzed showed similar results.

The mineral suspected to be either rutile or titanite based on observations made during polarization microscopy was identified as rutile. The data from all five grains analyzed in SEM-EDS matched with the data presented in Deer et al. (1963; Table 3). SEM images of the rutile grains analyzed can be found in Appendix 8.

EDS analyses of the opaque minerals observed in thin section, often together with rutile, were identified as ilmenite after comparing the results to Deer et al. (1963; Table 4). The two analysis points are of thin planar ilmenite inside rutile, believed to be exsolution lamellae. (for SEM images, see Appendix VIII).

4.4 Pressure-Temperature calculations

The P-T calculations of the three micro domains were made using the software GTB version 2.1, which was written by Kohn and modified by Spear in 1999. Based on the EDS analyses (Table 1), the assemblages Hbl + Grt and Grt + Pl + Hbl + Qtz were chosen, for geothermometry and geobarometry respectively. The results from the P-T calculations for each micro domain are shown in Fig. 11, and the calibrations used are specified with an identifying number. GTB can correct for Fe(3+), but since calculations based on Droop (1987) showed that none was present, all iron was assumed to be Fe(2+) and this correction was not made. Two geothermometers and six geobarometers were used. The geothermometer from Graham & Powell (1984) is based on the Fe and Mg exchange between hornblende and garnet, which can be represented by the exchange reaction

3 ferro-pargasite + 4 pyrope = 3 pargasite + 4 almandine

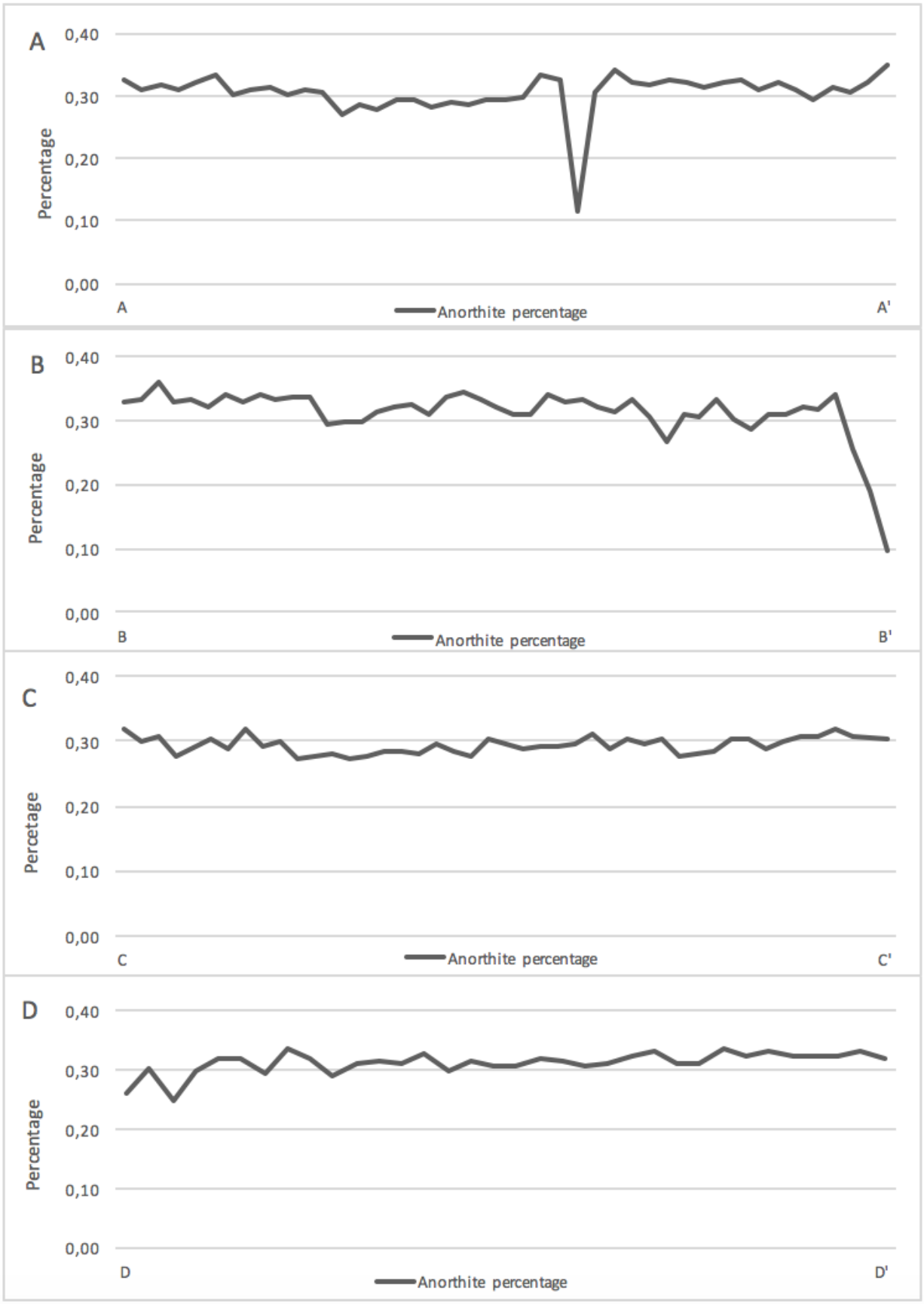

Fig. 9. Four profiles showing the anorthite content of plagioclase in thin section A. A and B are profiles through plagioclase in the matrix, C is a profile of plagioclase in a composite inclusion in garnet and D is plagioclase surrounding the rim of the garnet (where the rest of the matrix is located at D and the garnet rim is found by D').

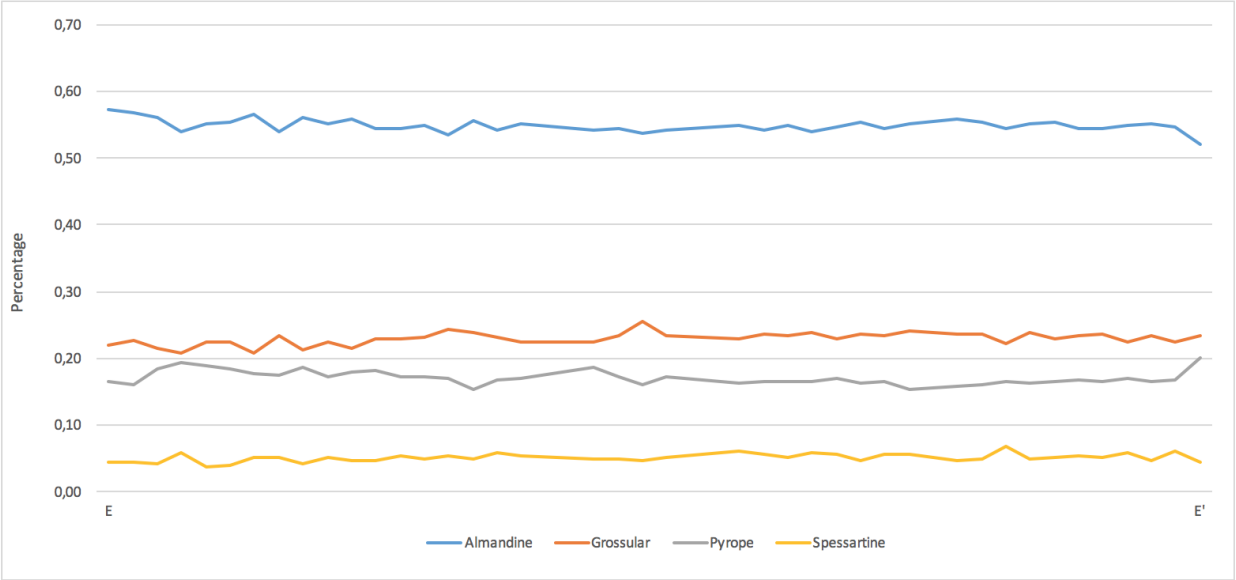

Figure 10. Profile across a garnet grain showing the contents of almandine, grossular, pyrope and spessartine. The profile was taken at the rim of the garnet in thin section A. Some analysis points were disregarded as their stoichiometry were not consistent. The garnet species andradite which contains Fe (III) is not included in the graph as Fe (III) was assumed to not be present, after calculations based on Droop (1987). The profile starts at E closer to the core of the garnet in a fracture and ends at E' by the rim of the garnet.

This calibration is called 1. Graham & Powell (1984). The geothermometer from Perchuk et al. (1985) is based, similarly to Graham & Powell (1984), on the Fe-Mg-exchange between hornblende and garnet. The basic reaction is as follows

Mg in amphibole + Fe in garnet = Mg in garnet + Fe in amphibole

This calibration is called 2. Perchuk et al. (1985). The geobarometers from Kohn & Spear (1989) are based on the equilibrium

6 anorthite + 3 albite + 3 tremolite = 2 grossular + 1 pyrope + 3 pargasite + 18 quartz

and its Fe end-member equivalent. These calibrations are 3. the Pargasite-Fe Model I, 4. the Pargasite-Mg Model I, 5. the Pargasite-Fe Model II and 6. the Pargasite-Mg Model II. The geobarometers from Kohn & Spear (1990) are based on the reactions

6 anorthite + 3 tremolite = 2 grossular + 1 pyrope + 3 tschermakite + 6 quartz

6 anorthite + 3 Fe-actinolite = 2 grossular + 1 al-

Table 2. Below, on the right: Microprobe analyses of alteration in biotite, which after comparing results with Deer, Howie and Zussman (1963) was found to be prehnite (Prh). The alternations were analyzed in two separate biotite grains, four analyze points in the first grain, Prh (1), and two points in grain two, Prh (2).

	Ilm (1)	Ilm (2)
TiO_2	52.39	53.53
FeO	45.56	44.92
Total	97.96	98.45
Ti	1.01	1.02
Fe	0.98	0.95
Cation sum	1.99	1.98
O	3	3

Table 4. Microprobe analyses of opaque mineral found inside of rutile grains. The stoichiometry corresponds to that of ilmenite (Deer et al 1962). The oxide total does not add up to 100, most likely because MgO was not included.

	Prh (1)	Prh (1)	Prh (1)	Prh (1)	Prh (2)	Prh (2)
SiO_2	42.49	43.53	42.33	42.34	42.67	43.08
Al_2O_3	21.73	22.32	21.58	21.73	22.47	22.49
MgO	0.03		0.16	0.09		
FeO	3.53	3.28	3.7	3.38	3.13	2.79
CaO	26.04	26.63	26.37	26.91	26.58	26.68
Total	93.82	95.76	94.15	94.46	94.86	95.04
Si	6.61	6.63	6.58	6.56	6.56	6.6
Al	3.98	4	3.95	3.97	4.07	4.06
Mg	0.01		0.04	0.02		
Fe	0.46	0.42	0.48	0.44	0.4	0.36
Ca	4.34	4.34	4.39	4.47	4.38	4.38
Cation sum	15.4	18.47	15.44	15.46	15.41	15.38
Oxygen	24	24	24	24	24	24

Table 3. Microprobe analyses of five rutile (Rt) grains in thin section A. It was not possible to determine if the mineral was rutile or titanite in polarisation microscope, but SEM-EDS analysis showed that it was rutile.

	Rt 1	Rt 2	Rt 3	Rt 4	Rt 5
TiO_2	99.39	99.18	99.32	99.23	99.65
Total	99.39	99.18	99.32	99.23	99.65
Ti	1	1	1	1	1
Cation sum	1	1	1	1	1
Oxygen	2	2	2	2	2

mandine + 3 Fe-tschermakite + 18 quartz

These calibrations are 7. the Tschermakite-Fe Model and 8. the Tschermakite-Mg Model.

Of the three micro domains analyzed, two were located by the rim of the garnet. The third micro domain was located near the core of the garnet. The two P-T diagrams made based on EDS analysis of the rim of the garnet showed fairly similar results. The calculations for micro domain 1 suggest temperatures between 680 and 720°C and pressures between 9 and 10 kbar, and for micro domain 2 temperatures around 700-750°C and pressures reaching 8.5-10 kbar (Fig. 11). The results from the P-T calculations for domain 3, which was located close to the core of the garnet, showed slightly lower temperatures reaching between 630 and 680°C and pressures around 9-10 kbar (Fig. 11).

5 Discussion

5.1 P-T conditions and metamorphic grade

Thermobarometry of the three micro domains analyzed in SEM-EDS indicate an increase of temperature as the garnet grew. The domain located close to the core of the garnet was formed under temperatures ranging from 630 to 680°C and pressures reaching 9-10 kbar. The two domains found by the rim of the garnet showed slightly higher temperatures reaching between 680 and 750°C and pressures ranging from 8.5 to 10 kbar. When studying the EDS data, the main difference in composition between the rim and the core was the Fe-amount in Hbl. It was considerably lower in the core, with the number of Fe-ions being 1.87 compared to 2.15 and 2.19 by the rim (Table 1).

Figure 12 shows the results from thermobarometry overlain on a diagram of the metamorphic facies. When the results were to be compared to facies, two geobarometers were first removed. These were the Kohn & Spear (1990) Tschermakite-Fe and Tschermakite-Mg Models. The four geobarometers of Kohn & Spear (1989) were assumed to be more accurate for

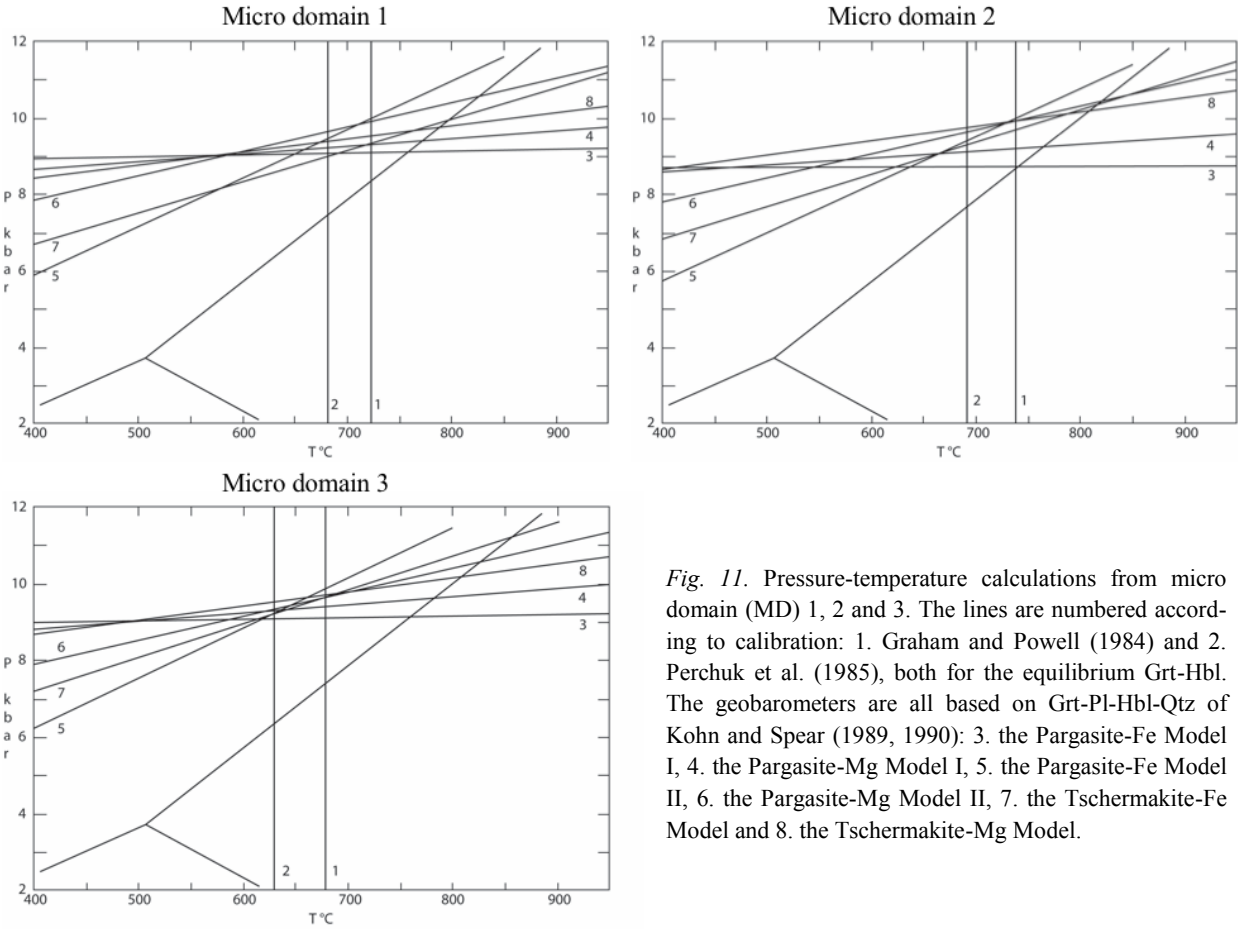

Fig. 11. Pressure-temperature calculations from micro domain (MD) 1, 2 and 3. The lines are numbered according to calibration: 1. Graham and Powell (1984) and 2. Perchuk et al. (1985), both for the equilibrium Grt-Hbl. The geobarometers are all based on Grt-Pl-Hbl-Qtz of Kohn and Spear (1989, 1990): 3. the Pargasite-Fe Model I, 4. the Pargasite-Mg Model I, 5. the Pargasite-Fe Model II, 6. the Pargasite-Mg Model II, 7. the Tschermakite-Fe Model and 8. the Tschermakite-Mg Model.

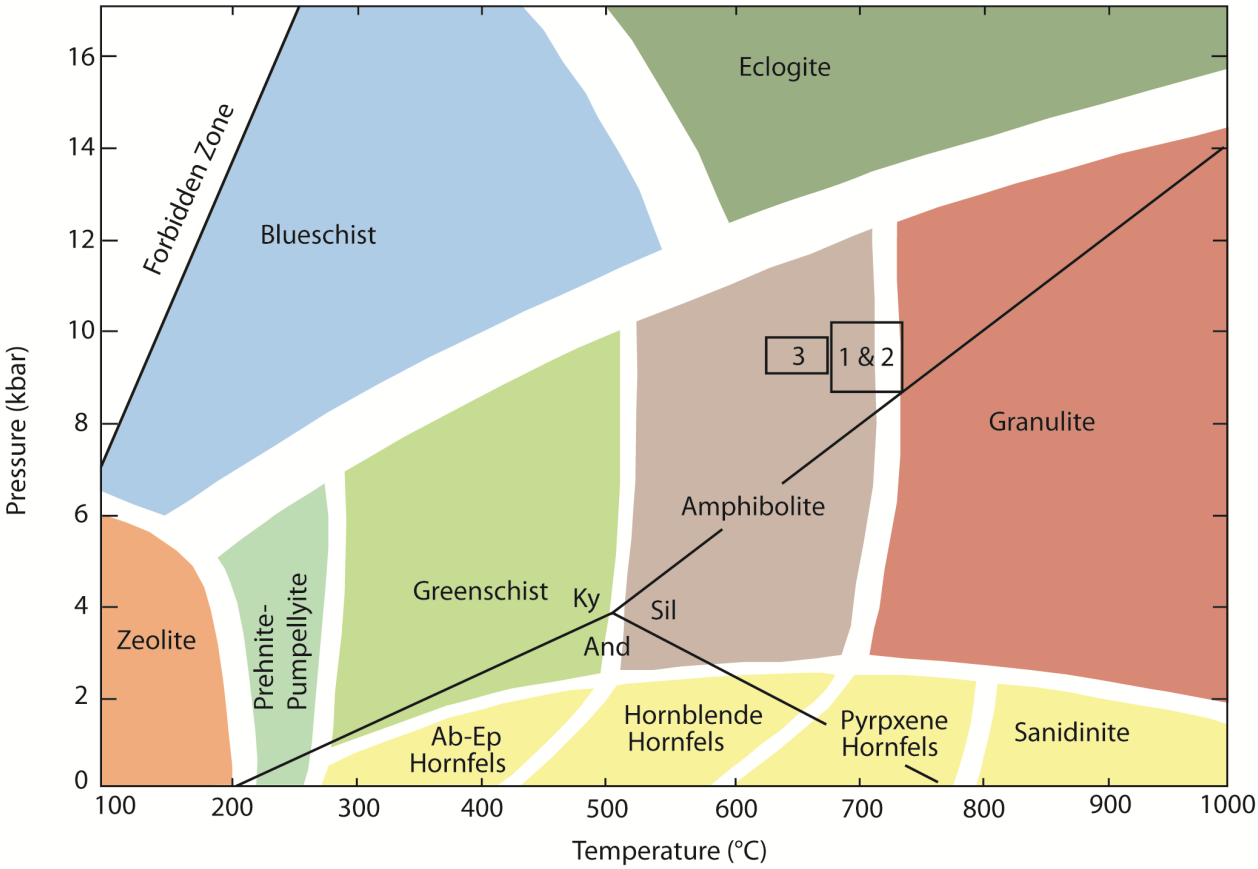

Fig. 12. Pressure-temperature diagram based on Winter (2014), with results from thermobarometry using the software GTB for micro domains 1, 2 and 3. The results from the three analyzed micro domains are marked as squares on the diagram. The metamorphic facies corresponding to various pressure and temperature conditions have been drawn to give a better overview of the placement of our micro domains. The P-T conditions of micro domains 1 and 2 overlap and have therefore been merged to one square. These two domains were both located at the rim of the garnet in thin section A. Micro domains 3 is located in the center of the garnet in the same thin section. The phase diagram of the aluminum silicates kyanite, sillimanite and andalusite has been drawn into the diagram and shows that the garnet amphibolite is located in the field where the polymorph kyanite is stable.

our sample, as they are based on pargasite which is compositionally closer to the analyzed amphibole (intermediate between edenite and pargasite/magnesiohastingsite). After comparing the results of the remaining calibrations with the facies in Figure 12, the garnet porphyroblast in thin section A was found to have formed in upper amphibolite facies.

The Idefjorden Terrane was buried to a depth of c. 35 km during the beginning of the Agder phase (1080-980 Ma), with high-pressure metamorphism reaching amphibolite- to granulite-facies (Bingen et al. 2008b; Ingered 2019). The pressures obtained from thermobarometry of the garnet amphibolite sampled in the Median Segment at the Hälltorp locality, indicates burial between 31.5 and 37 km. These depths as well as the metamorphic facies the amphibolite formed under, further suggests that the garnet grew during the Agder phase. This correlates well with U-Pb dates from migmatites sampled in the same area; Ingered (2019) found the age of migmatite crystallization in Median Segment gneisses to be 1019±27 Ma.

However, amphibolite-facies metamorphism and migmatization along the Mylonite Zone and the Göta Älv Shear Zone was dated at 0.98-0.97 Ga by Andersson et al. (2002), so there has been movement along these shear zones also during the Falkenberg phase.

5.2 Evidence of partial melting

Several migmatized garnet amphibolites were observed at the same locality as our sample was taken. Some of these were easy to identify according to the classification of Mehnert (1968), such as migmatites with net-like structures, dilation structures, schlieren structures and agmatitic migmatites. However, the amphibolite body sampled could not easily be classfied using Mehnert (1968), but the rims and tails observed suggested that partial melting might have occurred. It was thought a possible alternative, based on the lighter colored rims found surrounding the garnets. However, these could also have been formed as the garnet grew and depleted the surrounding melt of available elements so that only plagioclase and quartz could crystallize. The observations made in thin section gave a more detailed view of what the rock has undergone. The lighter colored rims consisted of plagioclase and quartz, and plagioclase was often located closest to the edge of the garnet as a thin rim (Fig. 13). Quartz and more plagioclase was then found as grains

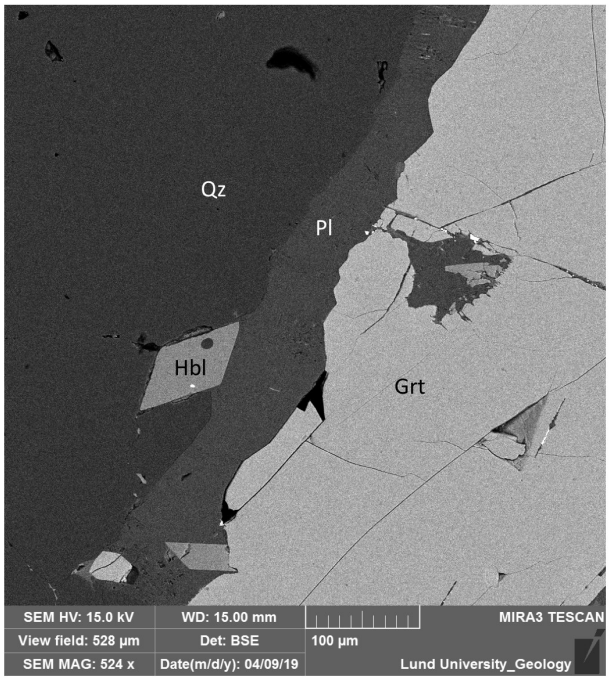

Fig. 13. SEM image showing the rim of the garnet in thin section A, with a thin rim of plagioclase surrounding it. Euhedral to subhedral hornblende grains can be found both in direct contact with the garnet and by the edge of the plagioclase rim. Quartz is found outside of the plagioclase. This is the location of the plagioclase profile D in Fig. 9.

surrounding it. Hornblende was in some locations found as small euhedral grains in the rim, which suggests that the lighter colored rim was not formed due to depletion of the melt as the garnet grew, but rather as a result of partial melting (Fig. 13). Hornblende consists of many of the elements needed to form garnet, and if depletion had occurred hornblende would not be likely to form. Plagioclase and quartz were also found as the dominant minerals instead of amphibole in two larger domains as well as a few smaller ones in thin section C. These areas where located in the matrix and were not in contact with the garnet porphyroblast (Fig. 4, thin section C). The occurrence of these two minerals in this manner suggests that partial melting has indeed occurred in this garnet amphibolite. Migmatization is therefore considered the more likely explanation. Furthermore, the thermobarometry showed that this rock has been under sufficient temperatures for partial melting to be able to occur. According to Winter (2014), partial melting of mafic rocks occurs at around 650-700 °C, under high pressures (8-10 kbar) and in the presence of H_2O. As the probable melt consists dominantly of quartz and plagioclase, the composition of the melt would be described as tonalitic. Composite inclusions in garnet consisting of Qtz + Pl indicates that the first growth of garnet occurred in the presence of partial melt. This suggests that the partial melt is a part of the high-grade metamorphic paragenesis and that all metamorphic minerals formed at the same time as partial melting occurred.

5.3 Evidence of equilibrium conditions

When discussing whether the studied garnet amphibolite records peak metamorphic conditions, it is first important to assess whether the texture and mineral compositions represent chemical equilibrium. According to Barker (1990), a rock records equilibrium if all phases are compatible with given pressure, temperature and fluid conditions and are arranged in the most stable, low energy configuration. Since the garnet amphibolite actually shows not only evidence of one but two metamorphic grades, the complete assemblage is not in equilibrium. The rock shows signs of local retrogression, with biotite being replaced by prehnite

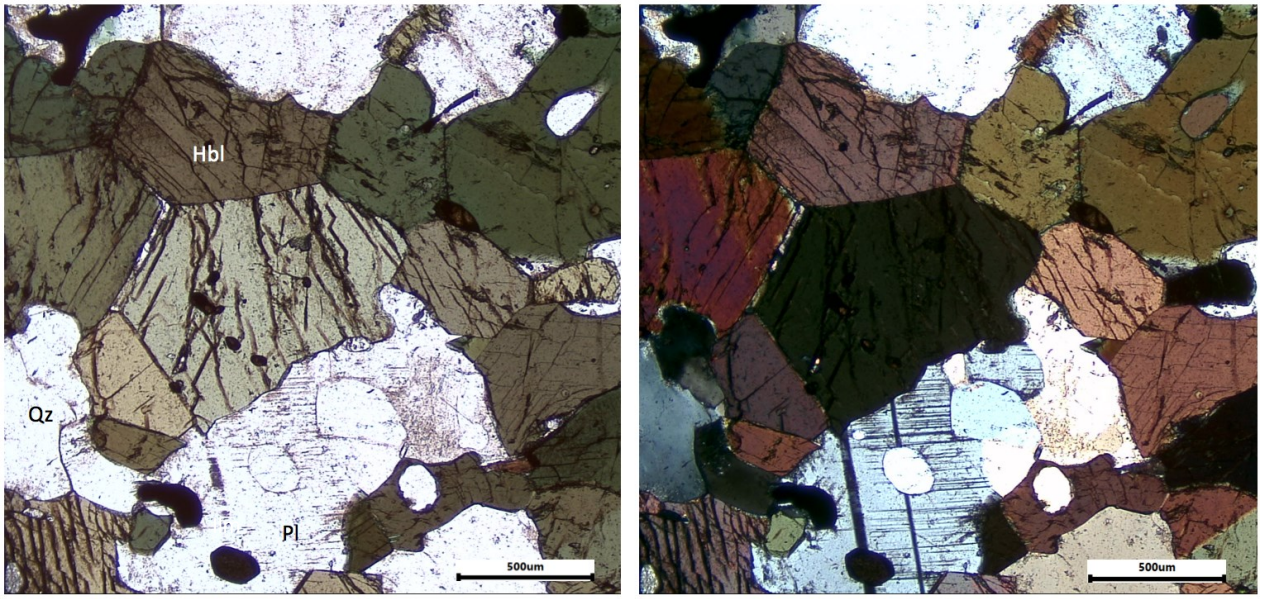

Fig. 14. Photos of thin section B taken with a camera attached to the polarization microscope. Straight grain boundaries of hornblende grains meeting in triple junctions can be seen in PPL (left) and in XPL (right). Weakly sericitized plagioclase, quartz and ilmenite can also be observed in the thin section.

and plagioclase being sericitized, but the other phases that represents higher grade metamorphism appear fresh and unaltered. Therefore, this section will discuss if the high- grade phases formed during equilibrium and not take into account the late retrograde alterations.

Best (1982) lists various observations that can indicate stable equilibrium in metamorphic paragenesis and some of these were found in our thin sections (Fig. 4; Fig. 14). A limited number of mineral species were found; these are hornblende, garnet, plagioclase, quartz, biotite, rutile, ilmenite, and zircon. All phases are observed to be in mutual contact with one another, which is another indication of equilibrium. There is a lack of zoning in the garnet, and also other minerals, such as plagioclase, are fairly compositionally homogenous (Appendix IIa, b, c). Barker (1990) also mentions that recrystallization leads to the grain structure and grain boundaries being modified in order to minimize the energy of the system. If recrystallization is complete, the assemblage has been modified to suit the pressure, temperature and fluid conditions present and the unit is in equilibrium. Barker (1990) also mentions that recrystallization often favors larger grains, and that smaller grains are commonly amalgated into larger ones. This results in a relatively uniform grain size. The observations made in the garnet amphibolite; a matrix consisting of relatively large, even-sized grains, indicates that the assemblage was close to equilibrium during peak metamorphism (Best 1982). The appearance of sharp, straight grain boundaries meeting in triple junctions and the polygonal structure of amphibolite grains, also suggests that this is a fairly stable arrangement of grains which formed close to equilibrium (Fig. 14). The textures and grain structure observed in the rock indicates conditions close to equilibrium. The fabric of the rock is isotropic which could indicate recrystallization in a low-strain site.

5.4 Rutile and ilmenite

In polarization microscopy and SEM-EDS, rutile and ilmenite were commonly observed together. In thin section B, a rutile grain that still contains a core of ilmenite was observed (Fig. 6). The two minerals are most commonly found in amphiboles in the matrix, but has also been found in plagioclase. Rutile has also been observed to be in direct contact with the accessory mineral zircon.

Before microprobe analysis was made, it was not known if these crystals were indeed rutile or titanite. Both minerals commonly form in metamorphic rocks by replacement of ilmenite (Angiboust & Harlov 2017). Experiments conducted by Angiboust and Harlov (2017) showed that ilmenite tends to recrystallize into rutile under higher pressures and into titanite during lower pressure metamorphism. The pressure boundary found for granitoid compositions was between 12 and 14 kbar. However, they also noted that for more low-Ca compositions, rutile appeared to be stable within ilmenite pseudomorphs as far down as 7 kbar. The pressures calculated for our sample ranged between 8.5 to 10 kbar. The relatively low amount of Ca found in plagioclase together with the recrystallization of ilmenite into rutile in our sample supports the experiments made by Angiboust and Harlov (2017). However, rutile was not found as ilmenite pseudomorphs, which suggests that for our specific composition and pressure combination, rutile is stable enough to begin to form as completely new crystals (Appendix VIII). Rutile being the high-pressure-high-temperature polymorph of TiO_2 is also mentioned by Deer et al. (1962). They also mention that rutile is the most commonly found polymorph in nature.

5.5 Low-grade alteration

Replacement of biotite by prehnite has previously been observed in the Kongsberg and Bamble Terranes (Field & Rodwell 1968). There, it was found most abundant in the migmatite zone and in major fault zones. The occurrence of prehnite in the garnet amphibolite at Hälltorp (Fig. 6; Fig. 15), studied herein, is also in an area with abundant migmatization. The field locality is also crossed by a NE-SW trending band of "strongly foliated rocks", as is marked on the geological map made by the Swedish Geological Survey (Fig. 3; Samuelsson & Lundqvist 1988). This could indicate a zone of higher strain in the bedrock.

Field & Rodwell (1968) describes that sericitized plagioclase is an essential constituent in observed rocks containing prehnite. This correlates well with our sample, in which local sericitization /saussuritization is present. In all observed cases of prehnite in the thin sections, it was found with sericitized plagioclase. Field & Rodwell (1968) describes the association

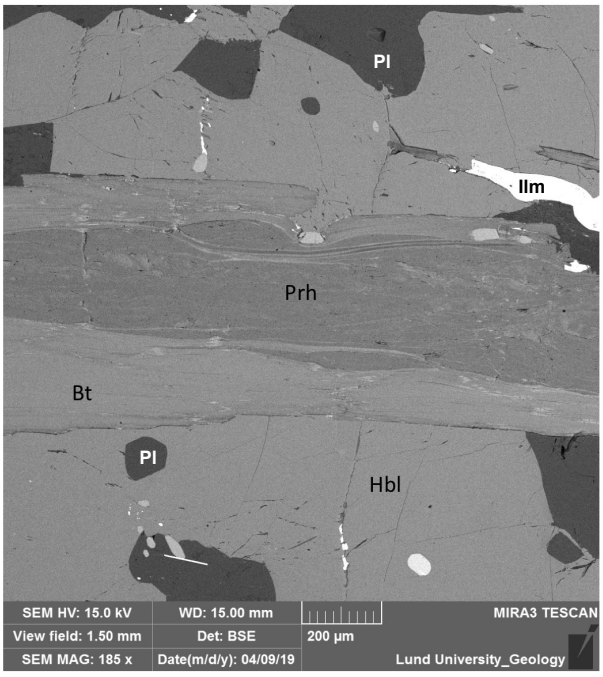

Figure 15. SEM image of prehnite replacing biotite in thin section A. The surrounding minerals seen are hornblende, plagioclase and ilmenite.

between sericite and prehnite as significant and states that the degree of sericitization and prehnitisation is related. In rocks where sericitization is complete, the majority of biotite grains contain prehnite. In the plagioclase-quartz dominated area found in thin section C, most of the plagioclase has been sericitized. Sericitized plagioclase was observed both in the matrix and in plagioclase inclusions in the garnet, but was more extensive in the former. Field & Rodwell (1968) suggests that prehnite has formed as a result of late stage hydrothermal sericitization, which allowed for Ca to be released into solution. Prehnite was crystallized in the closest suitable sites; the cleavage planes of biotite (Fig. 6; Fig. 15). The authors propose that the reaction occurred under relatively low pressures with a formation temperature ranging from 350 to 450°C (Field & Rodwell 1968) . It is plausible to believe that a similar reaction occurred also in our samples, since sericitized plagioclase and prehnite was found in such close proximity. The replacement of biotite by prehnite shows evidence of pumpellyite-prehnite facies, which together with chlorite growth is believed to be late alteration occurring after the peak metamorphism. It is therefore likely that the formation of prehnite occurred as the Median Segment was exhumed, most likely during the Dalene phase.

6 Conclusions

- P-T conditions during the formation of the amphibolite were in the ranges of 8.5 to 10 kbar and 630 to 750°C, which corresponds to the upper amphibolite facies and a depth of between 31.5 and 37 km. This is linked to the burial and heating of the Idefjorden Terrane during the Agder phase (1.08-0.98 Ga; Ingered 2019), since the terrane is believed to have reached a depth of at least 35 km during this time interval (Bingen et al. 2008b).
- The textures and grain structures found in the rock suggests that the high-grade phases formed close to equilibrium.
- The mineral domains containing quartz and plagioclase suggest that the garnet amphibolite underwent partial melting, and the occurrence of composite inclusions in garnet consisting of Qz + Pl suggests that partial melt is a part of the high-grade metamorphic paragenesis.
- The partial replacement of biotite by prehnite as well as local sericitization of plagioclase and chlorite growth provide evidence of local retrograde metamorphism at low pressures and temperatures, likely in the prehnite-pumpellyite facies (Fig. 12).

7 Suggestions for further research

- Analysis of P-T conditions in the Western Segment would enable an internal comparison within the Idefjorden Terrane, which in turn would give a better understanding of the evolution of the Sveconorwegian Orogen.
- Further examination of the garnet amphibolite found at Hälltorp with other geobarometers and geothermometers would help narrow down the P-T conditions and give a more statistically certain result.

8 Acknowledgements

I would like to sincerely thank my supervisor, Lotta Möller, who has offered support, enthusiasm and guidance throughout this project. I would also like to thank Leif Johansson for help with cutting and scanning of the sample, and Maria Herrmann for her assistance with GTB. Dino Leopardi Navarro and Anders Scherstén are thanked for their helpful discussions during polarization microscopy. Scherstén and Lena Lundqvist (SGU) are also thanked for their supervision during the field mapping campaign which lead to this study being possible. I am immensely grateful for Mimmi Ingered, who has been with me on this project from day one and who helped collect the sample. Field mapping would not have been the same without you, and I am thankful for your friendship, support and countless valuable discussions. Last, but far from least, I would like to thank Lykke Lundgren Sassner, Emmy Molin and Daan van den Broek, for their never-ending support.

9 References

Ahlin, S., Hegardt, A., E. & Cornell, D., 2006: Nature and stratigraphic position of the 1614 Delsjön augen granite-gneiss in the Median Segment of south-west Sweden. GFF 128:1, 21- 32.

Andersson, J., Möller, C. & Johansson, L., 2002: Zircon geochronology of migmatite gneisses along the Mylonite Zone (S Sweden): a major Sveconorwegian terrane boundary in the Baltic Shield. Precambrian Research 114, 121-147.

Angiboust, S. & Harlov, D., 2017: Ilmenite breakdown and rutile-titanite stability in metagranitoids; natural observations and experimental results. American Mineralogist 102, 1696–1708.

Barker, A. J., 1990: Introduction to metamorphic textures and microstructures. Blackie & Son Ltd, Glasgow. 162pp.

Beckman, V., Möller, C., Söderlund, U. & Andersson, J., 2017: Zircon Growth during Progressive Recrystallization of Gabbro to Garnet Amphibolite, Eastern Segment, Sveconorwegian Orogen. Journal of Petrology 58:1, 167-188.

Berthelsen, A. 1980: Towards a palinspastic tectonic analysis of the Baltic Shield. In Cogne, J. & Slansky, M. (eds.), Geology of Europe, from Precambrian to the post-Hercynian sedimentary basins 108, 5-21. Mémoires du B.R.G.M., Paris.

Best, M. G., 1982: Igneous and Metamorphic Petrology. W. H. Freeman and Company, New York.

630pp.
Bingen, B., Skår, Ø., Marker, M., Sigmond, E. M. O., Nordgulen, Ø., Ragnhildstveit, J., Mansfeld, J., Tucker, R. D. & Liégeois, J.-P., 2005: Timing of continental building in the Sveconorwegian orogen, SW Scandinavia. Norwegian Journal of Geology 85, 87-116.
Bingen B., Andersson, J., Söderlund, U. & Möller, C., 2008a: The Mesoproterozoic in the Nordic countries. Episodes 31, 1-6.
Bingen B., Nordgulen, Ø & Viola, G., 2008b: A four-phase model for the Sveconorwegian orogeny, SW Scandinavia. Norwegian Journal of Geology 88, 43-72.
Brewer, T. S., Åhäll, K.-I, Darbyshire, D. P. F, Menuge, J. F., 2002: Geochemistry of late Mesoproterozoic volcanism in southwestern Scandinavia: implications for Sveconorwegian/Grenvillian plate tectonic models. Journal of the Geological Society London 159, 129-144.
Deer, W. A., Howie, R. A. & Zussman, J., 1962: Rock-Forming Minerals: Non-Silicates, Vol. 5. Longmans, Green and Co LTD, London. 371pp (ilmenite, rutile
Deer, W. A., Howie, R. A. & Zussman, J., 1982: Rock-Forming Minerals: Orthosilicates, Vol. 1A. Geological Society of London. 919pp (prehnite)
Deer, W. A., Howie, R. A. & Zussman, J., 2001: Rock-Forming Minerals: Framework silicates, Feldspars, Vol. 4A. The Geological Society of London. Second edition. 972pp (plagioclase)
Droop, G. T. R., 1987: A general equation for estimating Fe3+ concentrations in ferromagnesian silicates and oxides from microprobe analyses, using stoichiometric criteria. Mineralogical Magazine 51, 431-435.
Eliasson, T. & Schöberg, H., 1991: U-Pb dating of the post-kinematic Sveconorwegian (Grenvillian) Bohus granite, SW Sweden: evidence of restitic zircon. Precambrian Research 51, 337-350.
Egerton, R.F., 2016: Physical Principles of Electron Microscopy: an introduction to TEM, SEM and AEM. 2nd edition. Springer, Cham. 196 pp.
Engvik, A. K., Bingen, B. & Solli, A., 2016: Localized occurrences of granulite: P–T modeling, U–Pb geochronology and distribution of early-Sveconorwegian high-grade metamorphism in Bamble, South Norway. Lithos 240-243, 84-103.
Field, D. & Rodwell, J. R., 1968: The occurrence of prehnite in a high grade metamorphic sequence from South Norway. Norsk Geologisk Tidsskrift 48, 55-59.
Goldstein, Joseph I., Newbury, Dale E., Michael, Joseph R., Ritchie, Nicholas W.M., Scott, John Henry J. & Joy, David C., 2018: Scanning Electron Microscopy and X-Ray Microanalysis, 4th edition. Springer, New York. 550 pp.
Graham, C. M. & Powell, R., 1984: A garnet-hornblende geothermometer: calibration, testing, and application to the Pelona Schist, Southern California. Journal of Metamorphic Geology 2, 13-31.
Gunnarsson, J. & Forsström, M., 2012: Tryck- och temperaturförhållanden under gotisk och svekonorvegiska metamorfos i Kosterskärgården. Dissertations in Geology at Gothernburg University B692, 1-58.
Hegardt, E. A., Cornell, D. H., Hellström, F. A. & Lundqvist, I., 2007: Emplacement ages of the mid-Proterozoic Kungsbacka Bimodal Suite, SW Sweden. GFF 129:3, 227-234.
Hernnäs, T., 2018: Garnet amphibolite in the internal Eastern Segment, Sveconorwegian Province: monitors of metamorphic recrystallization at high temperature and pressure during Sveconorwegian orogeny. Dissertations in Geology at Lund University 553, 1-36.
Hibbard, M. J., 1995: Petrography to petrogenesis. Prentice-Hall Inc., New Jersey. 587pp.
Hodges, K. V. & Spear, F. S., 1982: Geothermometry, geobarometry and the Al2SiO5 triple point at Mt. Moosilauke, New Hampshire. American Mineralogist 67, 1118-1134.
Ingered, M., 2019: Zircon U-Pb constraints on the timing of Sveconorwegian migmatite formation in the Western and Median Segments of the Idefjorden terrane, SW Sweden. Dissertations in Geology at Lund University 558, 1-76.
Johansson, L., Möller, C. & Söderlund, U., 2001: Geochronology of eclogite facies metamorphism in the Sveconorwegian Province of SW Sweden. Precambrian Research 106, 261-275.
Karlstedt, F., P-T estimation with theriak domino and Zr-in-titanite thermobarometry of Herrestad metabasite in S-W Sweden, Sveconorwegian orogeny. Dissertations in Geology at Lund University 520, 1-26.
Klein, C. & Philpotts, A., 2013: Earth Materials: Introduction to Mineralogy and Petrology. Cambridge University Press. 552pp.
Kohn, M. J. & Spear, F. S., 1989: Empirical calibration of geobarometers for the assemblage garnet + hornblende + plagioclase + quartz. American Mineralogist 74, 77-84.
Kohn, M. J. & Spear, F. S., 1990: Two new geobarometers for garnet amphibolites, with applications to southeastern Vermont. American Mineralogist 75, 89-96.
Leake, B. E., Woolley, A. R., Arps, C. E. S., Birch, W. D., Gilbert, M. C., Grice, J. D., Hawthorne, F. C., Kato, A., Kisch, H. J., Krivovichev, V. G., Linthout, K., Laird, J., Mandarino, J. A., Maresch, W. V., Nickel, E. H., Rock, N. M. S., Schumacher, J. C., Smith, D. C., Stephenson, N. C. N., Ungaretti, L., Whittaker, E. J. W. & Youxhi, G., 1997: Nomenclature of amphiboles: Report of the Subcommittee on amphibolites of the International Mineralogical Association, Commission on new minerals and mineral names. The Canadian Mineralogist 35, 219-246.
Mehnert, K. R., 1968: Migmatites and the Origin of

Granitic Rocks. Elsevier, New York. 394 pp.
Möller, C., 1998: Decompressed eclogites in the Sveconorwegian (-Grenvillian) orogen of SW Sweden: petrology and tectonic implications. Journal of Metamorphic Geology 16, 641-656.
Möller, C., 1999: Sapphirine in SW Sweden: a record of Sveconorwegian (Grenvillian) late-orogenic tectonic exhumation. Journal of Metamorphic Geology 17, 127–141.
Möller, C. & Andersson, J., 2018: Metamorphic zoning and behavior of an underthrusting continental plate. Journal of Metamorphic Geology 36, 567-589.
Möller, C., Andersson, J., Lundqvist, I., Hellström, F., 2007: Linking deformation, migmatite formation and zircon U-Pb geochronology in polymetamorphic orthogneisses, Sveconorwegian Province, Sweden. Journal of Metamorphic Geology 25, 727-750.
Möller, C., Andersson, J., Dyck, B. & Lundin, I. A., 2015: Exhumation of an eclogite terrane as a hot migmatitic nappe, Sveconorwegian orogen. Lithos 226, 147-168.
Park, R. G., Åhäll, K.-I. & Boland, M. P., 1991: The Sveconorwegian shear-zone network of SW Sweden in relation to mid-Proterozoic plate movements. Precambrian Research 49, 245-260.
Piñán Llamas, A., Andersson, J., Möller, C., Johansson, L. & Hansen, E., 2015: Polyphasal foreland-vergent deformation in a deep section of the 1 Ga Sveconorwegian orogen. Precambrian Research 265. 121-149.
Perchuk, L.L., Aranovich, L.Ya., Podlesskii, K.K., Lavrant'eva, I.V., Gerasimov, V.Yu., Fed'kin, V.V., Kitsul, V.I., Karsakov, L.P. & Berdnikov, N.V., 1985: Precambrian granulites of the Aldan shield, eastern Siberia, USSR. Journal of Metamorphic Geology 3, 265–310.
Samuelsson, L. & Lundqvist, I., 1988: Bedrock map 8B Vänersborg SO. Scale 1:50 000. Swedish Geological Survey, Af 160.
Sawyer, E.W., 2008: Atlas of Migmatites. The Canadian Mineralogist, Special Publication 9. NRC Research Press, Ottawa. 371 pp.
Slagstad, T., Roberts, N. M. W., Marker, M., Røhr, T. S. & Schiellerup, H., 2013: A non-collisional, accretionary Sveconorwegian orogen. Terra Nova 25, 30-37.
Slagstad, T., Roberts, N. M. W. & Kulakov, E., 2017: Linking orogenesis across a supercontinent; the Grenvillian and Sveconorwegian margins on Rodinia. Gondwana Research 44, 109-115.
Söderlund, P., 1999: Från gabbro till granatamfibolit: En studie av metamorfos i Åkermetabasiten vaster om Protoginzonen, Småland. Dissertations in Geology at Lund University 116, 1-22.
Söderlund, P., Söderlund, U., Gorbatschev, R. & Rodhe, A., 2004: Petrology and ion microprobe U-Pb chronology applied to a metabasic intrusion in southern Sweden: A study on zircon formation during metamorphism and deformation. Tectonics 23, 1-16.
Söderlund, U., Hellström, F. A. & Kamo, S. L., 2008: Geochronology of high-pressure mafic granulite dykes in SW Sweden: tracking the P–T–t path of metamorphism using Hf isotopes in zircon and baddeleyite. Journal of Metamorphic Geology 26, 539-560.
Tual, L., Piñán Llamas, A. & Möller, C., 2015: High-temperature deformation in the basal shear zone of an eclogite-bearing fold nappe, Sveconorwegian orogen, Sweden. Precambrian Research 265. 104-120.
Tual, L., Pitra, P. & Möller, C., 2017: P–T evolution of Precambrian eclogite in the Sveconorwegian orogen, SW Sweden. Journal of Metamorphic Geology, 35:5. 493-515.
Tual, L., Möller, C. & Whitehouse, M. J., 2018: Tracking the prograde P–T path of Precambrian eclogite using Ti-in- quartz and Zr-in-rutile geothermobarometry. Contributions to Mineralogy and Petrology 173:56. 1-15.
Winter, J. D., 2014: Principles of igneous metamorphic petrology. (2. ed.,). Pearson Education Ltd, Essex. 739pp.
Whitney, D. L. & Evans, B. W., 2010: Abbreviations for Names of Rock-Forming Minerals. American Mineralogist 95(1). p.185-187.
Åhäll, K.-I. & Connelly, J.N., 2008: Long-term convergence along SW Fennoscandia: 330 m.y. of Proterozoic crustal growth. Precambrian Research 163, 402-421.

Appendix I. Legend for bedrock map found in Fig. 3, modified from Samuelsson & Lundqvist (1988).

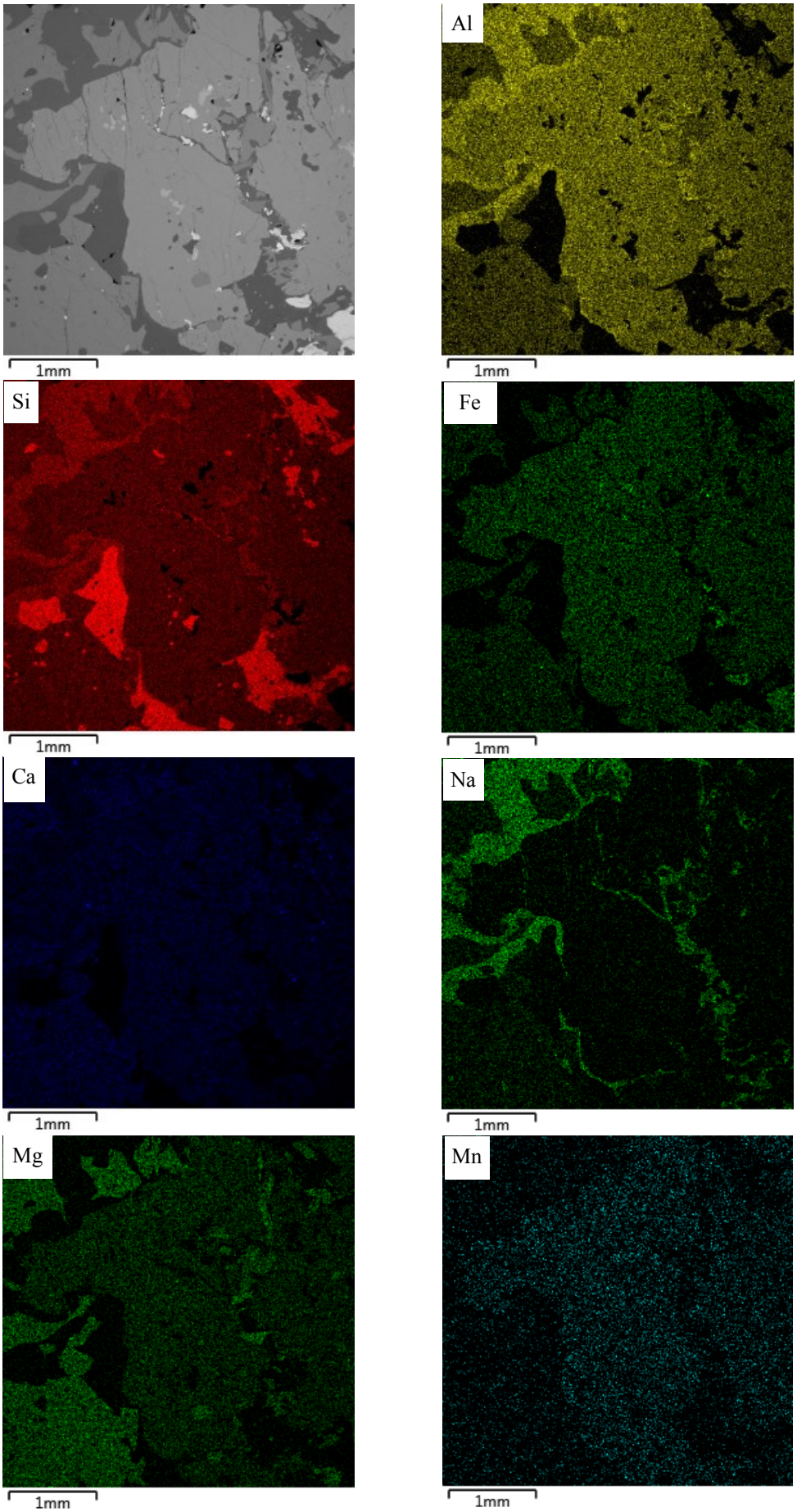

Appendix II.a. Elemental mapping of an area close to the rim of the garnet in thin section A., see Fig. 4. *Top left:* BSE image of the area mapped. The elements mapped were: Al, Si, Fe, Ca, Na, Mg and Mn.

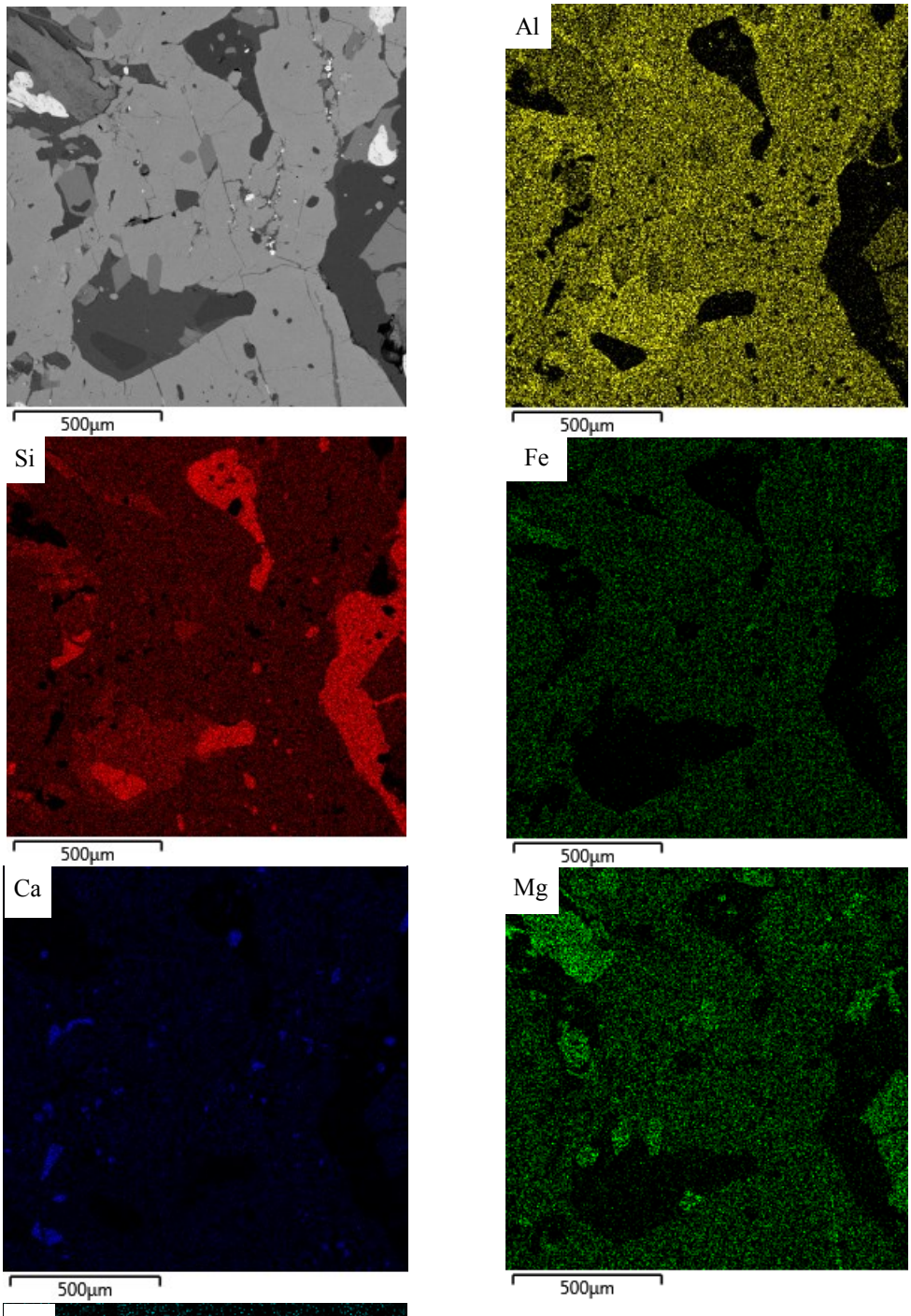

Appendix II.b. Elemental mapping of an area close to the core of the garnet in thin section A. *Top left:* BSE image of the area mapped. The elements mapped were: Al, Si, Fe, Ca, Mg and Mn.

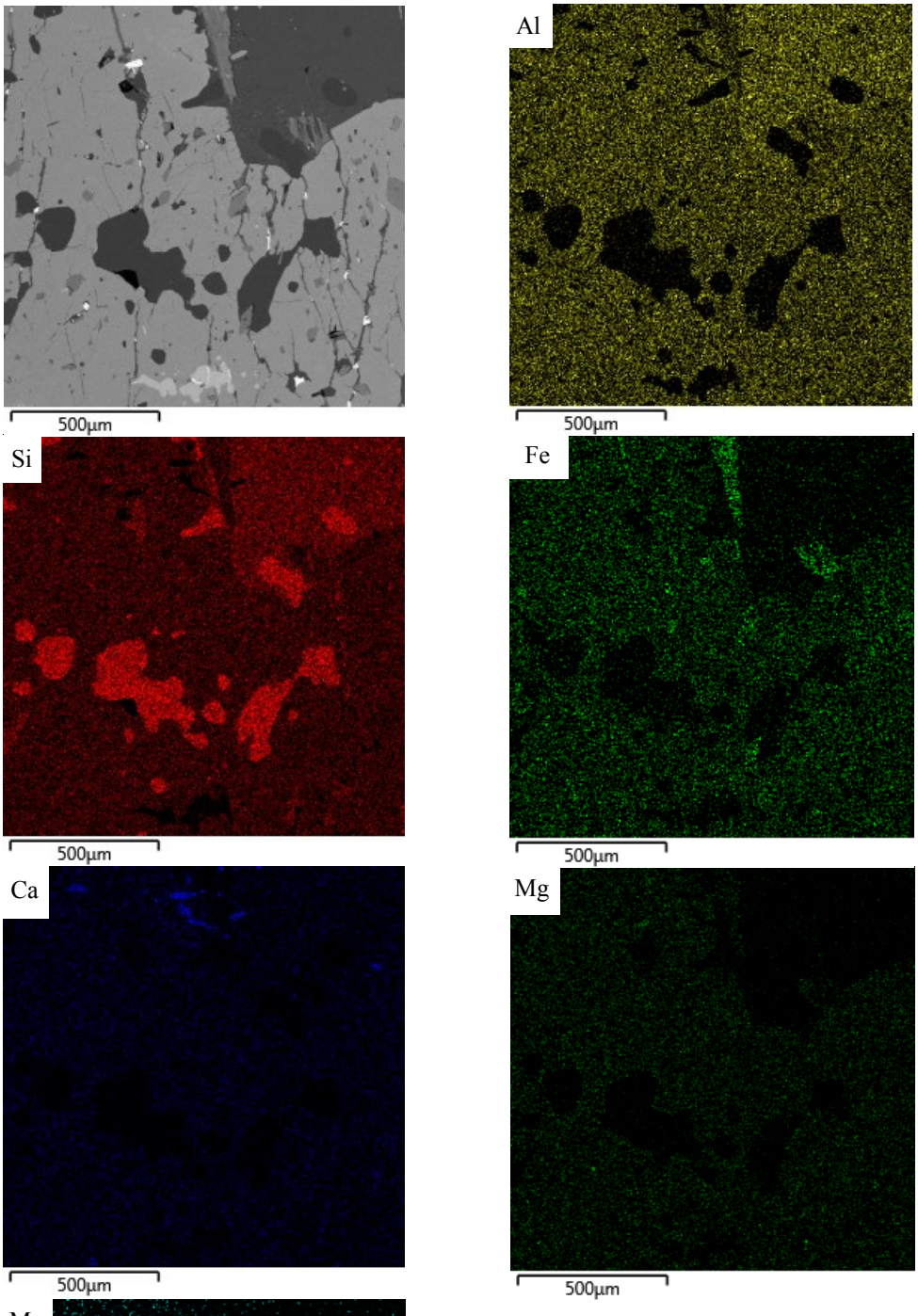

Appendix II.c. Elemental mapping of an area close to the rim of the garnet in thin section A., (see Fig. 4). *Top left:* BSE image of the area mapped. The elements mapped were: Al, Si, Fe, Ca, Na, Mg and Mn.

Appendix III. Table showing all EDS analyses made in micro domain 1, which is located at the rim of the garnet porphyroblast found in thin section A. The data has not been corrected for Fe (3+). Pl=plagioclase, Grt=garnet, Hbl=hornblende, according to Whitney & Evans (2010). Total values which are not within a margin of 2% error from the stoichiometrically correct value are marked in red.

	Micro domain 1																
	Pl					Grt								Hbl			
Al2O3	25,81	25,72	25,61	25,43	26,18	21,04	20,9	20,98	21,05	21,12	21,01	21,09	21,11	14,63	14,42	14,1	14,32	14,31
SiO2	58,5	58,96	58,77	58,32	57,89	37,23	37,29	37,35	37,5	37,61	37,28	37,52	37,8	39,81	40,44	40,35	40,56	41,09
FeO	0,13		0,21	0,13	0,15	25,08	25,73	25,47	25,58	25,8	25,36	25,43	25,1	17,02	17,25	17,14	17,01	16,92
CaO	7,22	7,23	7,01	7,15	7,73	7,83	7,82	7,9	7,83	7,57	7,83	7,74	7,88	10,75	10,79	10,95	10,93	11,1
Na2O	7,34	7,4	7,35	7,29	7									1,81	1,85	1,85	1,78	1,69
K2O														0,95	0,98	0,98	1,08	0,86
MgO						4,02	4,54	4,57	4,48	4,42	4	4,38	4,11	8,77	8,92	9	8,84	9,15
MnO						3,18	2,37	2,37	2,28	2,78	3,37	2,63	3,14	0,35	0,28	0,33	0,3	0,25
TiO2														1,33	1,43	1,48	1,44	1,39
Total	99,01	99,3	98,95	98,33	98,95	98,38	98,65	98,64	98,72	99,3	98,85	98,78	99,15	95,43	96,36	96,19	96,26	96,76
Al	1,37	1,36	1,36	1,36	1,39	1,99	1,97	1,97	1,98	1,98	1,98	1,98	1,98	2,66	2,6	2,55	2,58	2,56
Si	2,64	2,65	2,65	2,65	2,61	2,98	2,98	2,98	2,99	2,99	2,98	2,99	3	6,15	6,18	6,19	6,2	6,23
Fe	0,01		0,01		0,01	1,68	1,72	1,7	1,7	1,71	1,7	1,69	1,67	2,2	2,21	2,2	2,18	2,15
Ca	0,35	0,35	0,34	0,35	0,37	0,67	0,67	0,68	0,67	0,64	0,67	0,66	0,67	1,78	1,77	1,8	1,79	1,8
Na	0,64	0,64	0,64	0,64	0,61									0,54	0,55	0,55	0,53	0,5
K														0,19	0,19	0,19	0,21	0,17
Mg						0,48	0,54	0,54	0,53	0,52	0,48	0,52	0,49	2,02	2,03	2,06	2,02	2,07
Mn						0,22	0,16	0,16	0,15	0,19	0,23	0,18	0,21	0,05	0,04	0,04	0,04	0,03
Ti														0,15	0,16	0,17	0,17	0,16
Cation sum	5	5	4,99	4,99	5	8,02	8,04	8,03	8,02	8,03	8,03	8,02	8,01	15,73	15,72	15,74	15,71	15,66
Oxygen	8	8	8	8	8	12	12	12	12	12	12	12	12	23	23	23	23	23

Appendix IV. Table showing all EDS analyses made in micro domain 2, which is located at the rim of the garnet porphyroblast found in thin section A. The data has not been corrected for Fe (3+). Pl=plagioclase, Grt=garnet, Hbl=hornblende, according to Whitney & Evans (2010). Total values which are not within a margin of 2% error from the stoichiometrically correct value are marked in red.

	Micro domain 2																
	Pl					Grt					Hbl						
Al2O3	25,35	25,42	25,67	25,34	25,22	21,56	21,52	21,33	21,2	20,56	13,12	12,94	12,71	12,73	12,54	12,8	12,19
SiO2	60,44	61,52	61,82	59,43	60,17	37,39	37,86	37,39	37,88	36,05	42,15	41,58	40,06	38,75	38,23	38,54	37,63
FeO	0,1	0,07	0,02	0,12	0,21	25,46	25,99	25,26	25,73	24,75	17,3	17,54	16,55	16,4	16,38	16,6	16,04
CaO	6,54	6,24	6,25	6,59	6,39	7,86	7,88	7,61	7,88	7,33	11,14	10,9	10,66	10,36	10,29	10,27	10,18
Na2O	7,92	8,26	8,19	7,71	8,01						1,66	1,64	1,71	1,7	1,74	1,74	1,65
K2O		0,01									0,78	0,85	0,82	0,96	0,93	1	0,84
MgO						4,41	4,44	4,58	4,79	4,37	9,55	9,57	9,09	8,8	8,39	8,58	8,17
MnO						2,51	2,82	2,42	2,07	2,36	0,24	0,22	0,29	0,34	0,26	0,21	0,33
TiO2											1,12	1,18	1,1	1,13	1,16	1,32	1,06
Total	100,34	101,51	101,95	99,2	99,99	99,19	100,51	98,6	99,55	95,42	97,06	96,42	92,99	91,18	89,93	91,04	88,08
Al	1,32	1,31	1,32	1,34	1,32	2,02	1,99	2	1,97	2	2,34	2,33	2,37	2,43	2,43	2,45	2,41
Si	2,68	2,69	2,69	2,67	2,68	2,97	2,97	2,98	2,99	2,97	6,37	6,34	6,33	6,27	6,28	6,25	6,3
Fe					0,01	1,69	1,7	1,68	1,7	1,71	2,19	2,24	2,19	2,22	2,25	2,25	2,25
Ca	0,31	0,29	0,29	0,32	0,3	0,67	0,66	0,65	0,67	0,65	1,8	1,78	1,81	1,8	1,81	1,78	1,83
Na	0,68	0,7	0,69	0,67	0,69						0,49	0,49	0,52	0,53	0,55	0,55	0,54
K											0,15	0,17	0,16	0,2	0,2	0,21	0,18
Mg						0,52	0,52	0,54	0,56	0,54	2,15	2,18	2,14	2,12	2,05	2,07	2,04
Mn						0,17	0,19	0,16	0,14	0,16	0,03	0,03	0,04	0,05	0,04	0,03	0,05
Ti											0,13	0,14	0,13	0,14	0,14	0,16	0,13
Cation sum	5	5	4,99	5	5	8,03	8,03	8,02	8,03	8,03	15,65	15,68	15,7	15,75	15,74	15,74	15,72
Oxygen	8	8	8	8	8	12	12	12	12	12	23	23	23	23	23	23	23

Appendix V. Table showing all EDS analyses made in micro domain 3, which is located close to the center of the garnet porphyroblast found in thin section A. The data has not been corrected for Fe(3+). Pl=plagioclase, Grt=garnet, Hbl=hornblende, according to Whitney & Evans (2010).

	Micro domain 3																	
	Pl					Grt						Hbl						
Al2O3	25,4	24,82	24,77	25,06	24,64	21,37	21,65	21,51	21,27	21,5	21,27	13,94	13,79	14,06	14,04	13,96	13,98	
SiO2	59,17	59,76	59,82	59,34	60,01	38,45	38,08	38,14	37,84	37,68	37,33	41,45	41,95	41,93	41,85	42,36	42,03	
FeO	0,37	0,34	0,33	0,33	0,17	25,04	25,61	25,81	25,57	25,08	25,45	14,7	14,88	14,92	14,69	14,64	14,65	
CaO	6,72	6,21	5,96	6,44	6,28	8,12	8,07	7,88	8,01	7,71	7,81	11,4	11,09	11,22	11,15	11,24	11,03	
Na2O	7,61	7,81	7,95	7,71	8,02							1,62	1,72	1,69	1,67	1,59	1,63	
K2O												1,06	1,07	1,03	1	1,01	1,11	
MgO						4,8	4,84	4,82	4,82	4,62	4,72	10,67	10,72	10,7	10,7	11,14	11	
MnO						2,18	2,28	2,22	2,21	2,14	2,21	0,08	0,19	0,1	0,16	0,07	0,13	
TiO2												1,38	1,35	1,39	1,45	1,51	1,3	
Total	99,28	98,92	98,83	98,89	99,12	100,97	100,52	100,39	99,73	98,73	98,79	96,3	96,75	97,03	96,7	97,52	96,85	
Al	1,34	1,32	1,31	1,33	1,3	1,96	1,99	1,98	1,98	2,01	1,99	2,48	2,44	2,48	2,48	2,44	2,47	
Si	2,66	2,69	2,69	2,67	2,69	2,99	2,97	2,98	2,98	2,99	2,97	6,26	6,3	6,28	6,28	6,29	6,29	
Fe	0,01	0,01	0,01	0,01	0,01	1,7	1,67	1,69	1,68	1,66	1,69	1,86	1,87	1,87	1,84	1,82	1,84	
Ca	0,32	0,3	0,29	0,31	0,3	0,68	0,68	0,66	0,68	0,66	0,67	1,84	1,79	1,8	1,79	1,79	1,77	
Na	0,66	0,68	0,69	0,67	0,7							0,47	0,5	0,49	0,49	0,46	0,47	
K												0,21	0,2	0,2	0,19	0,19	0,21	
Mg						0,56	0,56	0,56	0,57	0,55	0,56	2,4	2,4	2,39	2,39	2,47	2,45	
Mn						0,14	0,15	0,15	0,15	0,14	0,15	0,01	0,02	0,01	0,02	0,01	0,02	
Ti												0,16	0,15	0,16	0,16	0,17	0,15	
Cation sum	5	4,99	5	5	5	8,03	8,03	8,03	8,03	8,01	8,03	15,68	15,68	15,57	15,65	15,64	15,67	
Oxygen	8	8	8	8	8	12	12	12	12	12	12	23	23	23	23	23	23	

Appendix VI. BSE images of the three micro domains. The upper photos are of the general area the analysis were made in and the lower ones show the specific areas analyzed. *Left:* micro domain 1, *middle:* micro domain 2, *right:* micro domain 3.

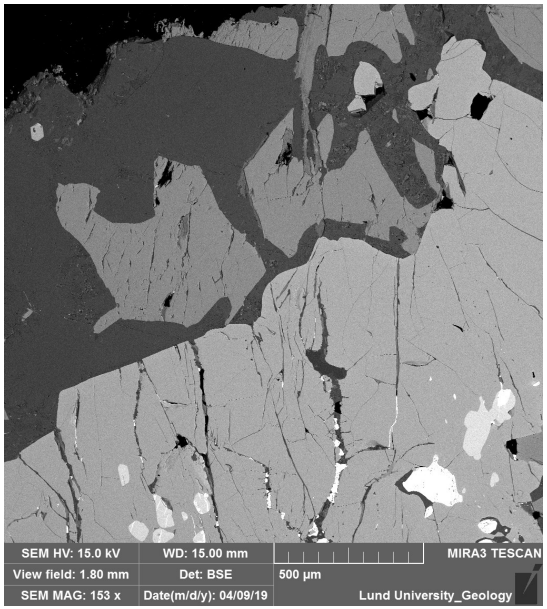

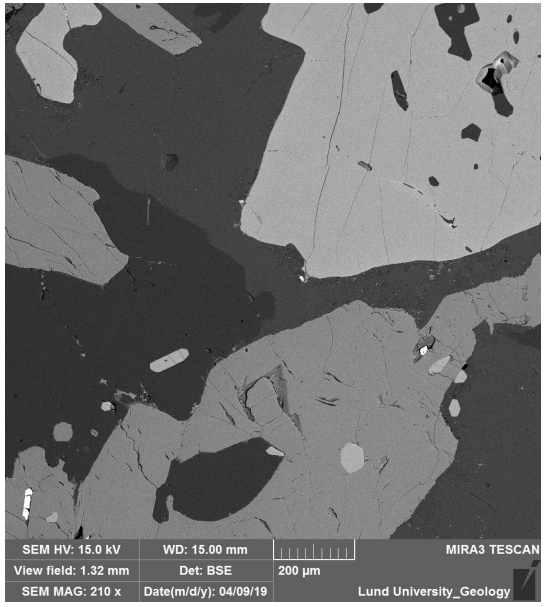

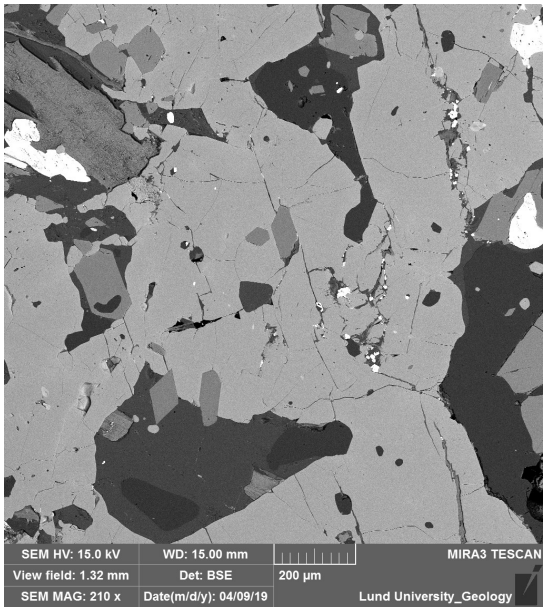

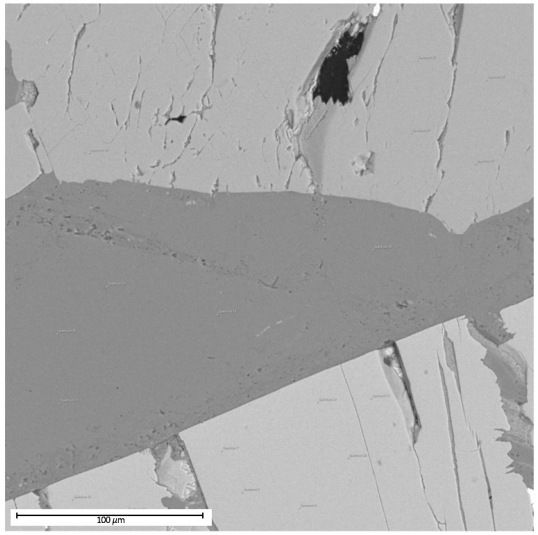

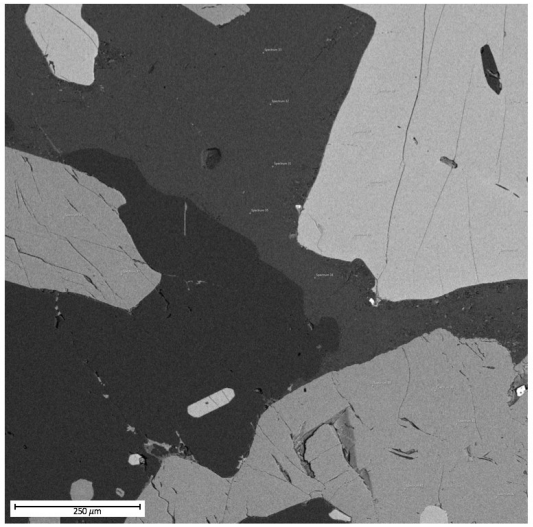

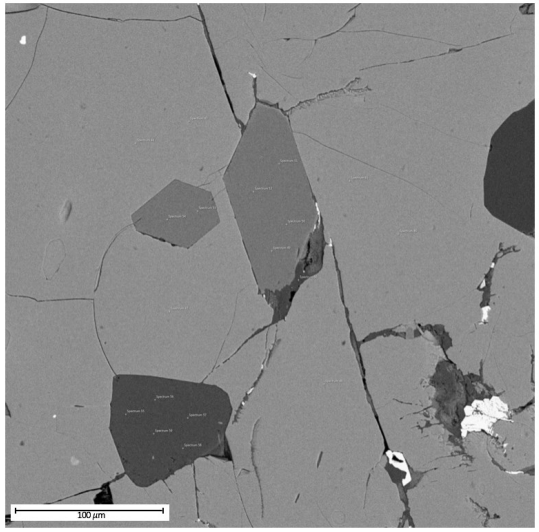

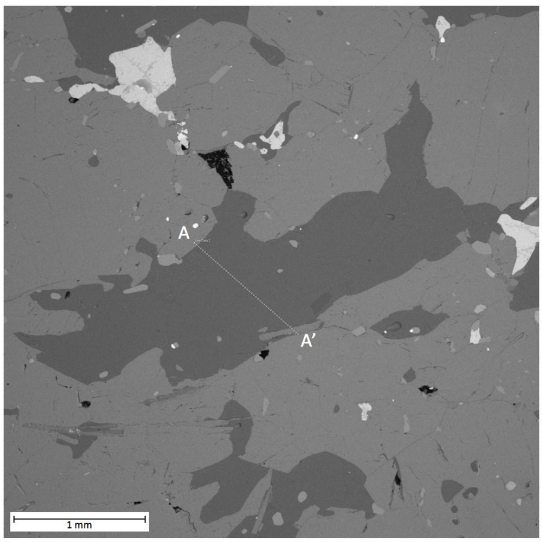

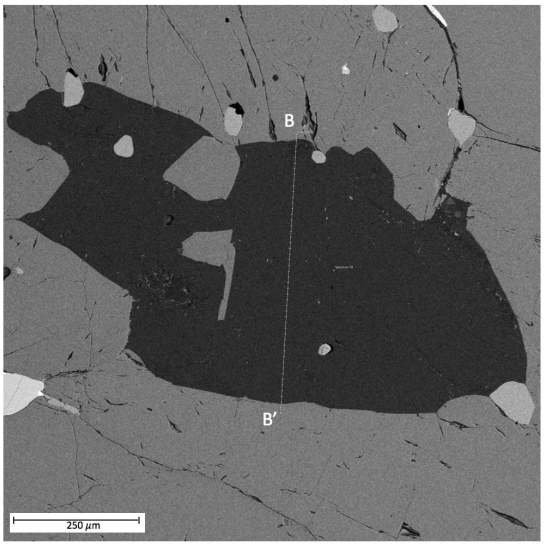

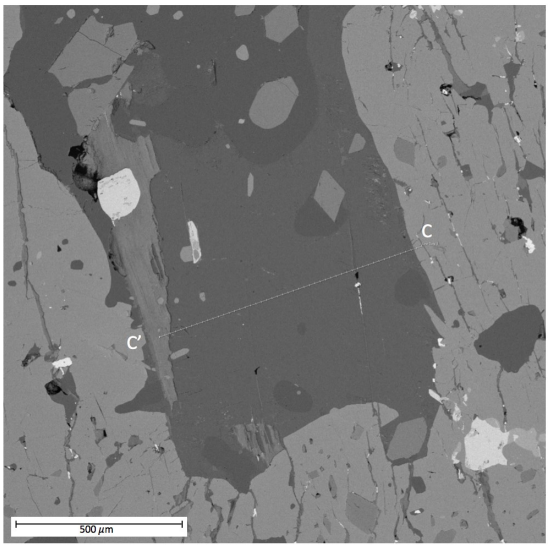

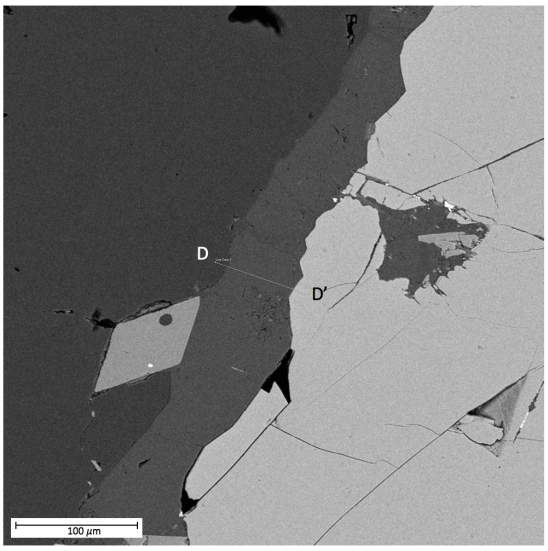

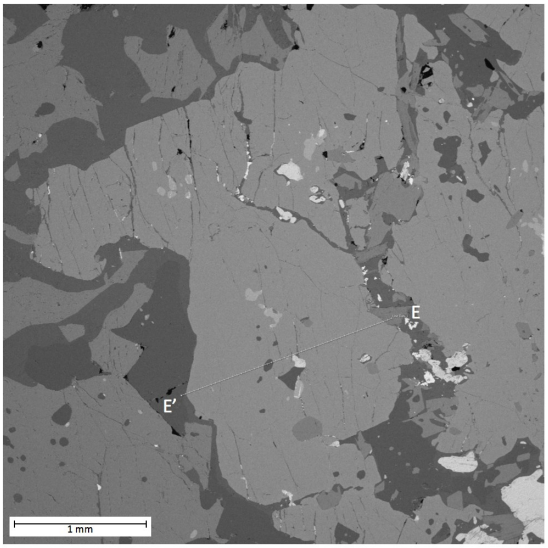

Appendix VII. BSE images showing the areas where profiles were made. The photos are marked with the letters found in the diagrams in Fig. 9 and 10. A-A', B-B', C-C' and D-D' are profiles of plagioclase and E-E' is a profile of the garnet porphyroblast.

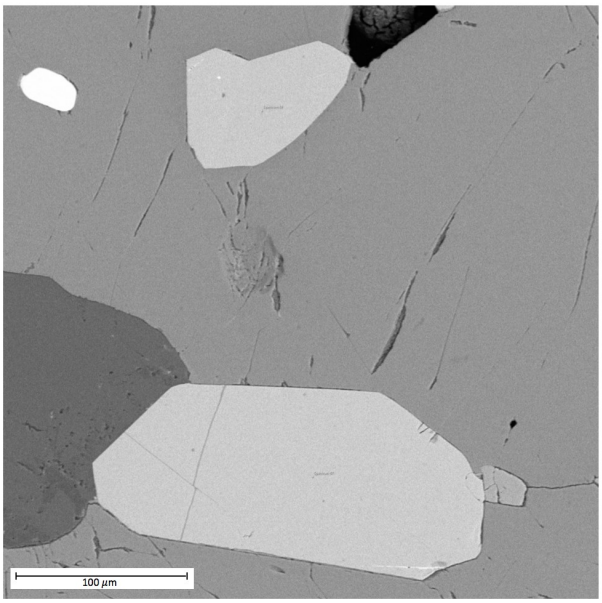

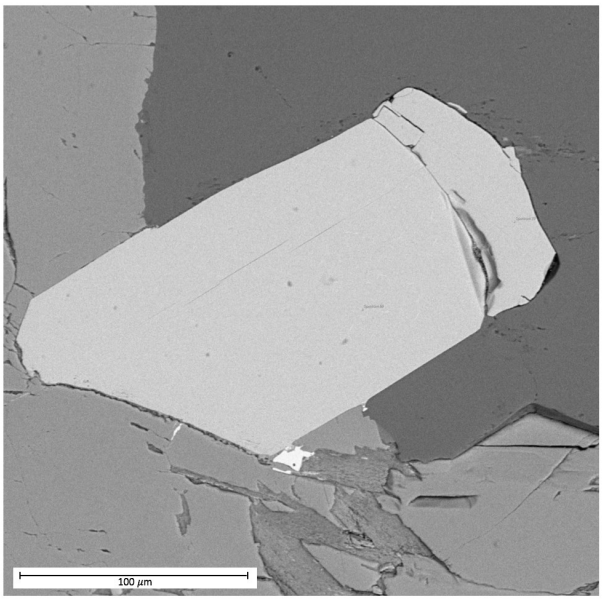

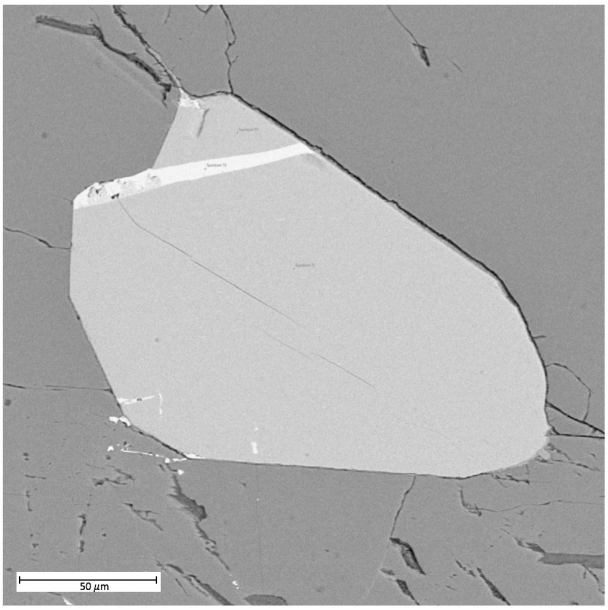

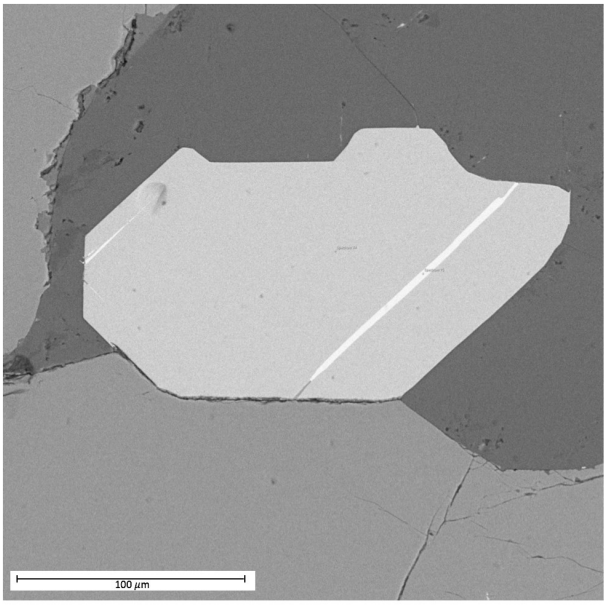

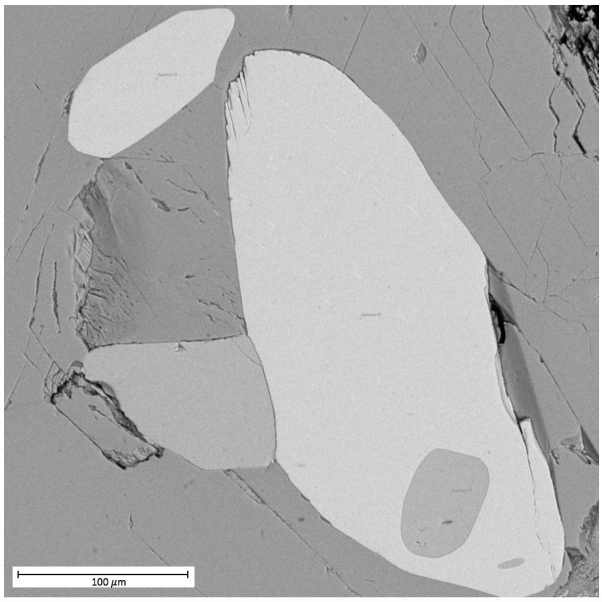

Appendix VIII. BSE images of analyzed grains of rutile with ilmenite exsolution. *Top left:* analysis point 1, *top right:* analysis point 2, *middle left:* analysis point 3, *middle right:* analysis point 4 and *bottom left*: analysis point 5.

Tidigare skrifter i serien ”Examensarbeten i Geologi vid Lunds universitet”:

519. Stjern, Rebecka, 2017: Hur påverkas luminiscenssignaler från kvarts under laboratorieförhållanden? (15 hp)
520. Karlstedt, Filippa, 2017: P-T estimation of the metamorphism of gabbro to garnet amphibolite at Herrestad, Eastern Segment of the Sveconorwegian orogen. (45 hp)
521. Önnervik, Oscar, 2017: Ooider som naturliga arkiv för förändringar i havens geokemi och jordens klimat. (15 hp)
522. Nilsson, Hanna, 2017: Kartläggning av sand och naturgrus med hjälp av resistivitetsmätning på Själland, Danmark. (15 hp)
523. Christensson, Lisa, 2017: Geofysisk undersökning av grundvattenskydd för planerad reservvattentäkt i Mjölkalånga, Hässleholms kommun. (15 hp)
524. Stamsnijder, Joaen, 2017: New geochronological constraints on the Klipriviersberg Group: defining a new Neoarchean large igneous province on the Kaapvaal Craton, South Africa. (45 hp)
525. Becker Jensen, Amanda, 2017: Den eocena Furformationen i Danmark: exceptionella bevaringstillstånd har bidragit till att djurs mjukdelar fossiliserats.(15 hp)
526. Radomski, Jan, 2018: Carbonate sedimentology and carbon isotope stratigraphy of the Tallbacken-1 core, early Wenlock Slite Group, Gotland, Sweden. (45 hp)
527. Pettersson, Johan, 2018: Ultrastructure and biomolecular composition of sea turtle epidermal remains from the Campanian (Upper Cretaceous) North Sulphur River of Texas. (45 hp)
528. Jansson, Robin, 2018: Multidisciplinary perspective on a natural attenuation zone in a PCE contaminated aquifer. (45 hp)
529. Larsson, Alfred, 2018: Rb-Sr sphalerite data and implications for the source and timing of Pb-Zn deposits at the Caledonian margin in Sweden. (45 hp)
530. Balija, Fisnik, 2018: Stratigraphy and pyrite geochemistry of the Lower–Upper Ordovician in the Lerhamn and Fågelsång -3 drill cores, Scania, Sweden. (45 hp)
531. Höglund, Nikolas, 2018: Groundwater chemistry evaluation and a GIS-based approach for determining groundwater potential in Mörbylånga, Sweden. (45 hp)
532. Haag, Vendela, 2018: Studie av mikrostrukturer i karbonatslagkäglor från nedslagsstrukturen Charlevoix, Kanada. (15 hp)
533. Hebrard, Benoit, 2018: Antropocen – vad, när och hur? (15 hp)
534. Jancsak, Nathalie, 2018: Åtgärder mot kusterosion i Skåne, samt en fallstudie av erosionsskydden i Löderup, Ystad kommun. (15 hp)
535. Zachén, Gabriel, 2018: Mesosideriter – redogörelse av bildningsprocesser samt SEM-analys av Vaca Muertameteoriten. (15 hp)
536. Fägersten, Andreas, 2018: Lateral variability in the quantification of calcareous nannofossils in the Upper Triassic, Austria. (15 hp)
537. Hjertman, Anna, 2018: Förutsättningar för djupinfiltration av ytvatten från Ivösjön till Kristianstadbassängen. (15 hp)
538. Lagerstam, Clarence, 2018: Varför svalde svanödlor (Reptilia, Plesiosauria) stenar? (15 hp)
539. Pilser, Hannes, 2018: Mg/Ca i bottenlevande foraminiferer, särskilt med avseende på temperaturer nära 0°C. (15 hp)
540. Christiansen, Emma, 2018: Mikroplast på och i havsbotten - Utbredningen av mikroplaster i marina bottensediment och dess påverkan på marina miljöer. (15 hp)
541. Staahlnacke, Simon, 2018: En sammanställning av norra Skånes prekambriska berggrund. (15 hp)
542. Martell, Josefin, 2018: Shock metamorphic features in zircon grains from the Mien impact structure - clues to conditions during impact. (45 hp)
543. Chitindingu, Tawonga, 2018: Petrological characterization of the Cambrian sandstone reservoirs in the Baltic Basin, Sweden. (45 hp)
544. Chonewicz, Julia, 2018: Dimensionerande vattenförbrukning och alternativa vattenkvaliteter. (15 hp)
545. Adeen, Lina, 2018: Hur lämpliga är de geofysiska metoderna resistivitet och IP för kartläggning av PFOS? (15 hp)
546. Nilsson Brunlid, Anette, 2018: Impact of southern Baltic sea-level changes on landscape development in the Verkeån River valley at Haväng, southern Sweden, during the early and mid Holocene. (45 hp)
547. Perälä, Jesper, 2018: Dynamic Recrystallization in the Sveconorwegian Frontal Wedge, Småland, southern Sweden. (45 hp)
548. Artursson, Christopher, 2018: Stratigraphy, sedimentology and geophysical assessment of the early Silurian Halla and Klinteberg formations, Altajme core, Gotland, Sweden. (45 hp)
549. Kempengren, Henrik, 2018: Att välja den mest hållbara efterbehandlingsmetoden vid sanering: Applicering av

beslutsstödsverktyget SAMLA. (45 hp)

550. Andreasson, Dagnija, 2018: Assessment of using liquidity index for the approximation of undrained shear strength of clay tills in Scania. (45 hp)
551. Ahrenstedt, Viktor, 2018: The Neoproterozoic Visingsö Group of southern Sweden: Lithology, sequence stratigraphy and provenance of the Middle Formation. (45 hp)
552. Berglund, Marie, 2018: Basaltkuppen - ett spel om mineralogi och petrologi. (15 hp)
553. Hernnäs, Tove, 2018: Garnet amphibolite in the internal Eastern Segment, Sveconorwegian Province: monitors of metamorphic recrystallization at high temperature and pressure during Sveconorwegian orogeny. (45 hp)
554. Halling, Jenny, 2019: Characterization of black rust in reinforced concrete structures: analyses of field samples from southern Sweden. (45 hp)
555. Stevic, Marijana, 2019: Stratigraphy and dating of a lake sediment record from Lyngsjön, eastern Scania - human impact and aeolian sand deposition during the last millennium. (45 hp)
556. Rabanser, Monika, 2019: Processes of Lateral Moraine Formation at a Debris-covered Glacier, Suldenferner (Vedretta di Solda), Italy. (45 hp)
557. Nilsson, Hanna, 2019: Records of environmental change and sedimentation processes over the last century in a Baltic coastal inlet. (45 hp)
558. Ingered, Mimmi, 2019: Zircon U-Pb constraints on the timing of Sveconorwegian migmatite formation in the Western and Median Segments of the Idefjorden terrane, SW Sweden. (45 hp)
559. Hjorth, Ingeborg, 2019: Paleomagnetisk undersökning av vulkanen Rangitoto, Nya Zeeland, för att bestämma dess utbrottshistoria. (15 hp)
560. Westberg, Märta, 2019: Enigmatic worm-like fossils from the Silurian Waukesha Lagerstätte, Wisconsin, USA. (15 hp)
561. Björn, Julia, 2019: Undersökning av påverkan på hydraulisk konduktivitet i förorenat område efter in situ-saneringsförsök. (15 hp)
562. Faraj, Haider, 2019: Tolkning av georadarprofiler över grundvattenmagasinet Verveln - Gullringen i Kalmar län. (15 hp)
563. Bjermo, Tim, 2019: Eoliska avlagringar och vindriktningar under holocen i och kring Store Mosse, södra Sverige. (15 hp)
564. Langkjaer, Henrik, 2019: Analys av Östergötlands kommande grundvattenresurser ur ett klimtperspektiv - med fokus på förstärkt grundvattenbildning. (15 hp)
565. Johansson, Marcus, 2019: Hur öppet var landskapet i södra Sverige under Atlantisk tid? (15 hp)
566. Molin, Emmy, 2019: Litologi, sedimentologi och kolisotopstratigrafi över krita–paleogen-gränsintervallet i borrningen Limhamn-2018. (15 hp)
567. Schroeder, Mimmi, 2019: The history of European hemp cultivation. (15 hp)
568. Damber, Maja, 2019: Granens invandring i sydvästa Sverige, belyst genom pollenanalys från Skottenesjön. (15 hp)
569. Lundgren Sassner, Lykke, 2019: Strandmorfologi, stranderosion och stranddeposition, med en fallstudie på Tylösand sandstrand, Halland. (15 hp)
570. Greiff, Johannes, 2019: Mesozoiska konglomerat och Skånes tektoniska utveckling. (15 hp)
571. Persson, Eric, 2019: An Enigmatic Cerapodian Dentary from the Cretaceous of southern Sweden. (15 hp)
572. Aldenius, Erik, 2019: Subsurface characterization of the Lund Sandstone – 3D model of the sandstone reservoir and evaluation of the geoenergy storage potential, SW Skåne, South Sweden. (45 hp)
573. Juliusson, Oscar, 2019: Impacts of subglacial processes on underlying bedrock. (15 hp)
574. Sartell, Anna, 2019: Metamorphic paragenesis and P-T conditions in garnet amphibolite from the Median Segment of the Idefjorden Terrane, Lilla Edet. (15 hp)

LUNDS UNIVERSITET

Geologiska institutionen
Lunds universitet
Sölvegatan 12, 223 62 Lund